The February–March 2000 Eruption of Hekla, Iceland from a Satellite Perspective

W. I. Rose[1], Y. Gu[1], I. M. Watson[1], T. Yu[1], G. J. S. Bluth[1], A. J. Prata[2], A. J. Krueger[3], N. Krotkov[3], S. Carn[3], M. D. Fromm[4], D. E. Hunton[5], G. G. J. Ernst[6], A. A. Viggiano[5], T. M. Miller[5], J. O. Ballenthin[5], J. M. Reeves[7], J. C. Wilson[7], B. E. Anderson[8], D. E. Flittner[9]

An 80,000 km^2 stratospheric volcanic cloud formed from the 26 February 2000 eruption of Hekla (63.98° N, 19.70° W). POAM-III profiles showed the cloud was 9–12 km asl. During 3 days this cloud drifted north. Three remote sensing algorithms (TOMS SO_2, MODIS & TOVS 7.3 μm IR and MODIS 8.6 μm IR) estimated ~0.2 Tg SO_2. Sulfate aerosol in the cloud was 0.003–0.008 Tg, from MODIS IR data. MODIS and AVHRR show that cloud particles were ice. The ice mass peaked at ~1 Tg ~10 hours after eruption onset. A ~0.1 Tg mass of ash was detected in the early plume. Repetitive TOVS data showed a decrease of SO_2 in the cloud from 0.2 Tg to below TOVS detection (i.e.<0.01 Tg) in ~3.5 days. The stratospheric height of the cloud may result from a large release of magmatic water vapor early (1819 UT on 26 February) leading to the ice-rich volcanic cloud. The optical depth of the cloud peaked early on 27 February and faded with time, apparently as ice fell out. A research aircraft encounter with the top of the cloud at 0514 UT on 28 February, 35 hours after eruption onset, provided validation of algorithms. The aircraft's instruments measured ~0.5–1 ppmv SO_2 and ~35–70 ppb sulfate aerosol in the cloud, 10–30% lower than concentrations from retrievals a few hours later. Different SO_2 algorithms illuminate environmental variables which affect the quality of results. Overall this is the most robust data set ever analyzed from the first few days of stratospheric residence of a volcanic cloud.

[1]Geological Engineering & Sciences, Michigan Technological University, Houghton, MI
[2]CSIRO, Atmospheric Research, Aspendale, Victoria, Australia
[3]JCET/UMBC, Baltimore, MD
[4]Computational Physics, Inc; Springfield, VA
[5]Air Force Research Laboratory, Space Vehicles Directorate, Hanscom AFB, MA
[6]CEGF, Earth Sciences, University of Bristol, UK
[7]Engineering Dept., University of Denver, CO
[8]NASA Langley Research Center, Hampton, VA
[9]University of Arizona, Tucson, AZ 85721

Volcanism and the Earth's Atmosphere
Geophysical Monograph 139

10.1029/139GM07

INTRODUCTION

This is a study of satellite remote sensing of a small stratospheric eruption using thermal infrared and ultraviolet sensors. The focus is the Hekla February 2000 eruption, the first explosive event studied with the MODIS instrument (http://modis.gsfc.nasa.gov/index.html). MODIS (Moderate Resolution Imaging Spectroradiometer) is a key instrument aboard the Terra (EOS AM) and Aqua (EOS PM) satellites. Other instruments used in this study include meteorological polar-orbiting multispectral IR sensors Advanced Very High Resolution Radiometer (AVHRR; http://www.ngdc.noaa.gov/seg/globsys/avhrr2.shtml) and High Resolution Infrared Radiation Sounder/TIROS Operational Vertical Sounder (HIRS-2/TOVS). AVHRR and HIRS/2 are carried on the same platforms and are favorably positioned for frequent imagery of polar

regions such as Iceland. We also used the Total Ozone Mapping Spectrometer (TOMS, http://skye.gsfc.nasa.gov/) which has already been shown to be sensitive to volcanic SO_2 (*Krueger et al.,* 1995), as well as data from the Polar Ozone Aerosol Measurement (POAM-III) instrument on the SPOT 4 spacecraft to constrain the height and width of the Hekla cloud. We have done this study to investigate MODIS' robust potential for volcanic cloud measurements and to compare its results with other sensors. The data from all sensors represent a comprehensive set of scientific data for an eruption, taking advantage of the synoptic satellite view. We also present some data collected in situ, following an accidental encounter with this volcanic cloud by a NASA research aircraft on February 28, 2000. These latter data represent a serendipitous chance for validating data for the various algorithms used in remote sensing of volcanic clouds.

Details of the Eruption and Hekla's Past

On 26 February 2000 at 1819 UT, an eruption of Hekla began, its 18th since European settlement about 876 AD [*Haraldsson et al., 2002*]. The eruption had an early energetic subplinian phase, which produced a dominantly white plume [*Good, 2001*]. At 1825 UT, radar observations show the eruption column reached 11 km asl and was carried north by light winds [*R Stefansson, GVN 25/2*]. Clear observations from the ground were prevented beyond the first 60 minutes of eruption due to severe blizzard conditions and rapidly settling darkness. Snow flakes falling at 2000 UT encased ash particles [*H Mattson, pers commun, 2002*]. Pilot reports to the Icelandic CAA [*S Kristjansson, pers comm, 2002*], real time seismic data and weather radar imagery [*S Karlsdóttir, pers comm, 2002*] indicate that the most intense explosive activity lasted several hours until about 2200 UT, after which the summit activity decreased to a level of intense fire fountaining and phreatomagmatic explosions in the summit area. At about 2200 UT the explosive activity stabilized to a low intensity and explosive activity ended entirely by 0500 UT on 27 February. Following this, a 4.5 km long fissure which opened on Hekla's ridge early in the eruption extruded lava flows until March 8, 2000 [*Ólafsdóttir et al., 2002; Hoskuldsson, pers comm, 2001*]. In all a total volume of about 0.17 km^3 of magma was erupted [*Ólafsdóttir et al., 2002*]. The explosive phase produced a tephra fallout deposit covering roughly 18,000 km^2 in a N direction with total volume estimated at 0.01 km^3 [*Haraldsson et al., 2002*]. By the morning of 27 February, the explosive phase had waned and effusive fissure activity dominated. The lava and ashfall composition was mainly basaltic andesite with an SiO_2 content of 54% (by weight). There was a small amount of dacite in the ashfall materials [*Hoskuldsson and Ólafsdóttir, 2002*].

The dynamics of Hekla's 2000 eruption qualitatively resembled 4 previous events in 1947–48 [*Thorarinsson, 1967*], 1970 [*Thorarinsson & Sigvaldason, 1972*], 1980–1 [*Gronvold et al., 1983*] and 1991 [*Gudmundsson et al., 1992*]. Each started with a prominent explosive phase which resulted in stratospheric venting of erupted materials and a tephra fallout deposit, followed by a more extended effusive period with fissure lavas, generally of basaltic andesite composition. The silicic Hekla dacite and rhyolite which occurs in Hekla's early plinian phases has been interpreted as being due to the partial melting of the Icelandic metabasic crustal materials by rising mantle-derived basalt which itself differentiates to produce basaltic andesite before eruption [*Sigmarsson et al., 1992*].

Hekla's plinian volcanic cloud of 1947–48 was described in detail by *Thorarinsson* [1967] as being mainly gas-rich and ash-poor based on photographs taken at that time, showing a white uppermost part of the plinian cloud. The 1970 Hekla volcanic cloud was actively sampled by aircraft [*Cadle & Blifford, 1971*] and it contained silicate glass shards with 55% SiO_2 and an abundance of sulfates and sulfuric acid. *Oskarsson* [1980] studied fluorine adsorption on Hekla's 1970 tephra, which poisoned surface water, and *Frogner et al.* [2001] studied the reactions between the 2000 ashfall and ocean water.

Data and Methods Used

The satellite data sets we examined are listed in Table 1. We used those data to map the position of the volcanic clouds at successive times and to make estimates of the various components (ash, ice, sulfate and SO_2). Various IR bands of interest in our studies are listed in Table 5. We used 11 and 12 μm wavelength IR data from AVHRR and MODIS to retrieve information about the optical depth of the volcanic cloud, the effective radius of ash or ice particles visible by the sensor [*Rose et al., 2000*] and the mass of fine ash or ice following the methods of *Wen & Rose* [1994] and *Rose et al.* [1995].

Three different methods are used to measure volcanic cloud SO_2. We used 7.3 μm wavelength IR data from MODIS and HIRS/2-TOVS [*Smith et al.,* 1979] for SO_2 burden determinations using the scheme of *Prata et al.* [2003]. With the 8.6 μm wavelength IR data available on MODIS, we used a scheme first developed by *Realmuto et al.* [1997] and employing atmospheric corrections applied via the MODTRAN radiative transfer code [*Berk et al.*

Table 1. Eruption details, satellite and aircraft data of this study.

Date	UT	sensors	retrievals, comments
2/26/00	**1819**		**onset of eruption**
〃	**1828**	**ground based radar**	**Top at 11 km asl**
〃	1945	AVHRR, TOVS	ash, ice, SO_2
〃	**~2000**	**pilot report to CAA**	**Cloud top at 10-12 km asl**
〃	2100	MODIS	ice
〃	2135	AVHRR	ice
〃	**2200**		**Decrease in eruption intensity**
2/27/00	0359	AVHRR	ice
〃	0547	AVHRR, TOVS	ice, SO_2
〃	**~0600**		**End of explosive activity**
〃	0737	AVHRR, TOVS	ice, SO_2
〃	0918	AVHRR,TOVS	ice, SO_2
〃	1108	AVHRR,TOVS	ice, SO_2
〃	1139	TOMS	SO_2, AI
〃	1236	AVHRR, TOVS	ice, SO_2
〃	1350	MODIS	ice, SO_2 (7.3, 8.6), sulfate
〃	1417	AVHRR, TOVS	ice, SO_2
〃	1557	AVHRR, TOVS	ice, SO_2
〃	1616	AVHRR, TOVS	ice, SO_2
〃	1740	AVHRR, TOVS	ice, SO_2
〃	2015	MODIS	ice, SO_2 (7.3, 8.6), sulfate
〃	2155	MODIS	ice, SO_2 (7.3, 8.6), sulfate
〃	2335	MODIS	ice, SO_2 (7.3, 8.6), sulfate
2/28/00	0359	AVHRR, TOVS	ice, SO_2
〃	**0508**	**DC8 encounter**	**CIMS data**
〃	0536	AVHRR, TOVS	ice, SO_2
〃	0706	AVHRR, TOVS	ice, SO_2
〃	1041	AVHRR, TOVS	ice, SO_2
〃	1115	MODIS	ice, SO_2 (7.3, 8.6), sulfate
〃	1200	TOMS	SO_2, AI
〃	1407	TOVS	SO_2
〃	1559	TOVS	SO_2

also see listing of TOVS data collected on 29 Feb and 1 Mar in Table 6.

1989] to estimate SO_2 burdens. We also estimated SO_2 burdens using the UV TOMS sensor, following the methods explained by *Krueger et al.* [1995].

For retrievals of the effective radius and masses of sulfate aerosols and ice, we used a multispectral IR scheme which is based on 7 MODIS thermal IR channels (27-33) and the method of *Yu & Rose* [2000], using the MODTRAN code and a lookup table for mixtures of ice and sulfate particles. Validation of all of these methods is sparse, and the Hekla data set represents the very first opportunity to compare and evaluate independent SO_2 retrievals on a given volcanic cloud. Moreover, there is independent validation information in this case because of the research aircraft encounter discussed hereafter.

The NASA DC-8 aircraft's great circle route from Edwards AFB, California USA, to Kiruna, Sweden, intercepted the Hekla volcanic cloud at an altitude of 11.3 km at about 75°N and 5°W between 0508 and 0518 UT on 28 February (Figure 1) about 1300 km NNE of Hekla. The position of the airplane at these times is shown as the thick line segment along the flight path. Before and after encountering the volcanic cloud trace gas and aerosol measurements were unperturbed. The intercept occurred 35 hours after the start of the eruption and its time with respect to all our measurements is given in Table 1. The volcanic cloud moved considerably between the time of the TOMS image and the DC-8 encounter, as our remote sensing data shows. The calculated plume crossing position matches our observations.

The DC-8 payload for the SOLVE (SAGE III Ozone Loss and Validation Experiment) mission consisted of 17 scientific instruments or suites of instruments [*Newman, 1999*]. Three

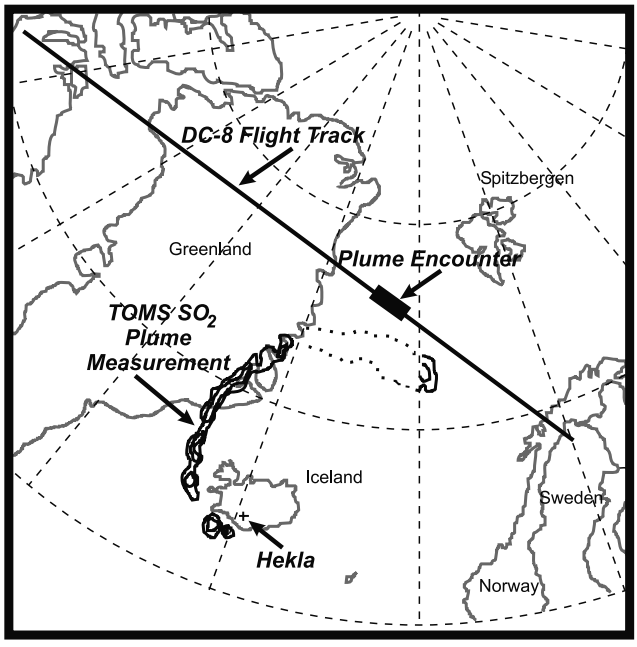

Figure 1. Map showing Hekla Volcano, the volcanic cloud as detected by TOMS on Feb. 27th, and the flight track of the NASA DC-8 aircraft on Feb. 28th.

of these are particularly important for the present comparison to remote sensing data. The Air Force Research Laboratory chemical ionization mass spectrometer (CIMS) [*Hunton et al., 2000; Talbot et al., 1999; Viggiano & Hunton, 1999; Miller et al., 2000*] was optimized to measure *in-situ* mixing ratios of HNO_3, SO_2, and HCN. The details of the operation of this instrument are reported elsewhere. For these gases, the instrument attained 20% accuracy, better than 10% precision, response times faster than 1 second, and detection sensitivities approaching 10 pptv. Concentrations of H_2SO_4, HCl, HF, and H_2S were obtained from less frequent full mass scans. The ion chemistry and instrument sensitivity for these gases were confirmed during post-mission laboratory calibrations. Here, only data on SO_2 and a limit on the amount of gas phase H_2SO_4 are reported since those species are important for comparison with the remote sensing data. Only a limit can be placed on gas phase H_2SO_4 due to the possibility of evaporation of aerosol H_2SO_4 in the inlet line.

Aerosol size measurements were made by the University of Denver Focused Cavity Aerosol Spectrometer (FCAS II) [*Jonsson et al., 1995*] and Nuclei-Mode Aerosol Size Spectrometer (N-MASS). The N-MASS detects particles in the diameter range 4 to 100 nm, while the FCAS II covers 90 to 2000 nm. Corrections were made for diffusion loss, instrument efficiencies, and departures from isokinetic sampling at the inlet. The combined measurements were then inverted to obtain the full aerosol size distribution from 4 to 2000 nm. The volatile and nonvolatile fractions of aerosol concentrations in various size bins were measured by the NASA Langley Particle Measurement System (PMS).

POAM III made observations of the Hekla volcanic cloud on February 29 and March 1, 2000. POAM measures solar extinction by the atmosphere using the solar occultation technique: the sun is observed through the Earth's atmosphere as it rises and sets as viewed from the satellite. POAM data have been applied to the study of Polar Mesospheric Clouds [*Debrestian et al., 1997*], and the study of Polar Stratospheric Clouds and stratospheric clouds of smoke traceable to boreal forest fires [*Fromm et al., 1997, 1999, 2000*]. In this paper the POAM cloud height determinations were especially important.

SATELLITE SENSING OF VOLCANIC CLOUD ICE

Thermal infrared sensors are routinely used to map clouds. At 10 μm wavelength cloud outlines are well-detected day and night. If they are optically thick and in the troposphere, their radiances and temperatures correlate inversely with cloud height. Thus cloud patterns may be mapped and the heights of clouds estimated. Meteorological clouds with temperatures less than –15°C usually contain appreciable numbers of ice crystals, while supercooled liquid water cannot exist in clouds below –40°C [*Rogers & Yau, 1989*]. In the earliest images of the Hekla eruption (Figure 2) the Hekla volcanic cloud spreads as a partially bifurcating plume and wind blown cloud [*Ernst et al., 1994*]. It extends from the volcano, spreading laterally under gravity while being advected downwind to the NE and drifting N. Brightness temperatures of this plume were –55° to –70°C which matches the temperature values of 7–13 km asl that day (tropopause temperatures were –60 to –65 °C at 9.5–10 km) as measured by radiosonde (from stations at Keflavik, and in Greenland and Jan Mayan).

Many eruption clouds have been mapped and discriminated using brightness temperature differencing (BTD) methods [*Prata, 1989a, b*], where volcanic ash absorbs and scatters upwelling infrared energy from under the volcanic cloud differently than water droplets or ice. Silicate particles absorb and scatter more strongly than water or ice at 10 μm while ice and water absorb and scatter more at 11 μm. Thus in a dry atmosphere BTD differencing shows clouds dominantly laden with ash with BTD < 0 while clouds dominantly laden with with liquid water or ice particles have BTD > 0 [*e.g. Wen & Rose, 1994*]. Apart from the first image at 1945 UT, which shows some regions with weakly negative BTD, the 2000 Hekla volcanic clouds show nearly always BTD > 0, and

because they also have BT < –40°C, we interpret them to be clouds dominantly laden with ice. The expectation at temperatures colder than –22 °C (at least down to –50 °C which is closest to the temperatures measured here) is that the habit of the ice crystals, which is extremely temperature dependent above –22 °C, should be dominantly prism-like hollow columns [*Wallace & Hobbs, 1977*]. Such strongly non-spherical shapes will affect retrievals for mass [*Krotkov et al., 1999a; Krotkov et al., 1999b*] and perhaps especially so as platy or elongated ice particles may become preferentially oriented in the radial electric fields around lightning flashes [*Foster & Hallett, 2002*].

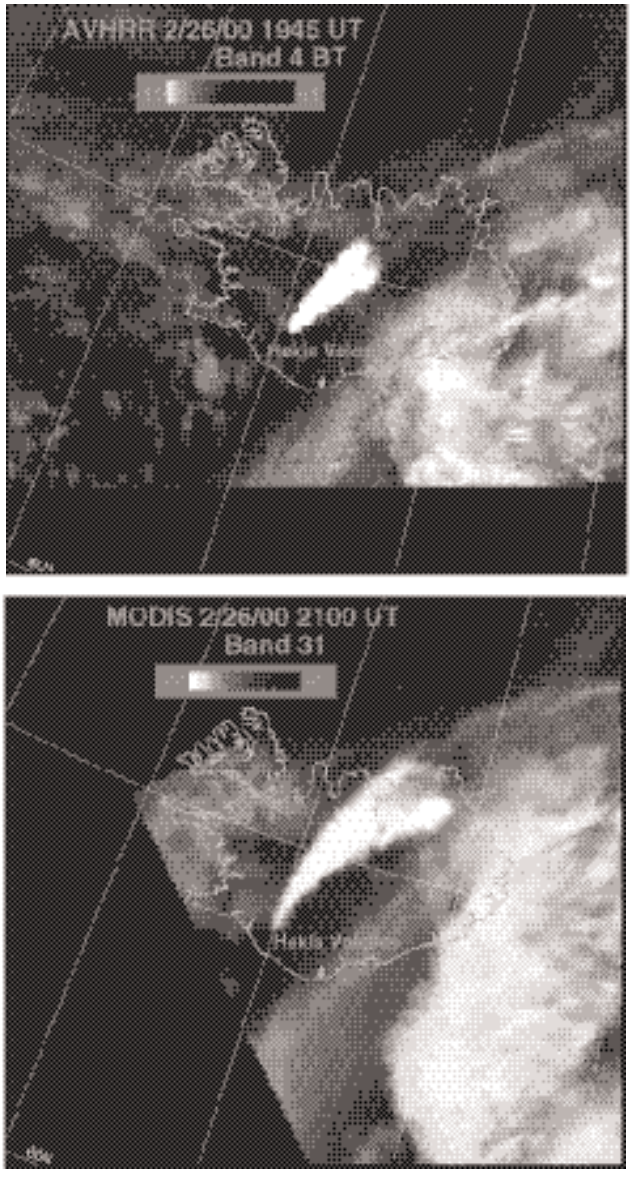

Figure 2. Satellite images from the first 3 hrs of the Hekla eruption, showing an active plume rising to stratospheric levels (brightness temperatures <–65°C) and continuously venting from Hekla. Above is AVHRR at 1945 UT band 4 (10.7 μm) BT, below is MODIS band 31 (10.7 μm) BT. Bright colors are cold temperatures, and black is warm according to the bar legend. Note ash cloud bifurcation visible at the leading edge (see *Ernst et al.* [1994] for discussion of the origin of this type of structure).

We have detected ice previously in volcanic clouds at Rabaul in 1994 [*Rose et al., 1995*] and at Montserrat in 1997 [*Mayberry et al., 2002*]. The Hekla volcanic clouds showed strong positive BTD (up to +10 or more) which made them stand out on BTD plots for more than 24 hours after eruption and emplacement in the stratosphere. The strength of the BTD signal depends on the temperature contrast between the cloud and its underlying surface. In the Hekla case, the tropopause height of the Hekla volcanic clouds results in a strong temperature contrast with the Atlantic Ocean and lower- level meteorological clouds. Thus in the thermal IR, the Hekla clouds resembled cirrus clouds.

Only in the first image we studied, at 1945 on 26 February, did we observe any portion of the volcanic cloud to have BTD < 0 (Figure 2). The high optical depth interior of the cloud had weakly negative BTD, consistent with a larger ash than ice contribution to the IR retrievals. We did separate ash retrievals for the interior of the 1945 cloud (ash) and for its outer regions (ice). The expectation is that while coarse ash particles were falling out quickly the finer ash particles remaining in the cloud were serving as nuclei for ice growth. These processes are also inferred for the Rabaul plume studied by *Rose et al.* [1995] and ice and snow-encased ashfalls (from a 9 km high cloud) were also directly documented from the ground during the 1963 eruption of Surtsey, Iceland [*Thorarinsson, 1965*]. The mass of fine ash retrieved for the interior of the Hekla cloud is estimated to be ~ 100 kilotonnes or 0.1 Tg. Because the net BTD signal represents combined abundances of ash and ice particles, because the ash cloud has only a short atmospheric residence and would be likely to contain substantial amounts of particles too large to be retrieved by Mie scattering and because many or most ash particles may have been encased in ice, the ash estimate is likely only a small fraction of the real ash mass in the Hekla cloud.

Figure 3 and Plates 2 and 3 show the cloud maps of BTD and Table 3 shows the results of retrievals of ice masses and particle effective radii for successive times during the 42 hours following the Hekla eruption. The mass of detected ice increased fastest during the first 3 hours after eruption onset (corresponding to an injection rate of 10^6 kg/s), then increased by about 10% over the next 7 hours, peaking at ~1.1 Tg after about 10 hours of atmospheric residence, and

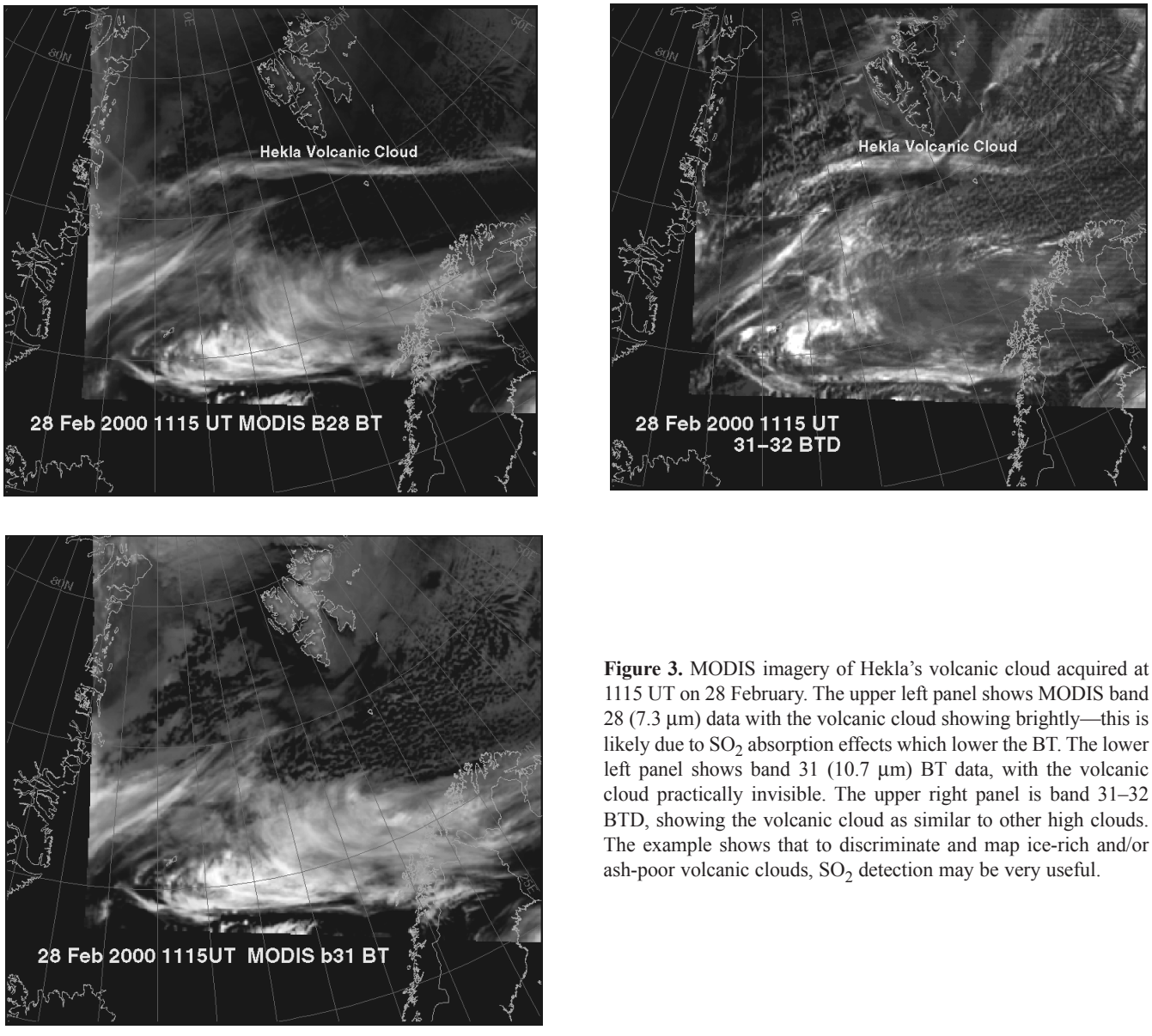

Figure 3. MODIS imagery of Hekla's volcanic cloud acquired at 1115 UT on 28 February. The upper left panel shows MODIS band 28 (7.3 μm) data with the volcanic cloud showing brightly—this is likely due to SO_2 absorption effects which lower the BT. The lower left panel shows band 31 (10.7 μm) BT data, with the volcanic cloud practically invisible. The upper right panel is band 31–32 BTD, showing the volcanic cloud as similar to other high clouds. The example shows that to discriminate and map ice-rich and/or ash-poor volcanic clouds, SO_2 detection may be very useful.

then declined by a factor of three in 12 hours (Table 3; Figure 6). The Hekla clouds moved gradually to the north, being deformed by storm systems. By the 28th of February, ~36 hours after eruption, the Hekla cloud no longer stands out in a BTD image (Figures 5 and 6) but the cloud is prominent in MODIS band 28 BT (at ~7.3 μm, Figure 6a), suggesting that it was by then dominated by SO_2.

SATELLITE SO_2 MEASUREMENTS

We were able to map the Hekla cloud clearly with 3 independent satellite SO_2 detection schemes: 8.6 μm SO_2 (Plate 4), 7.3 μm SO_2 (Plate 5) and Earth Probe TOMS SO_2 (Plate 6). We also were able to compare mass estimates of SO_2 from the various methods for the first time (Tables 2, 4). The mapped results show that SO_2 sensing was an excellent way to track the Hekla cloud, especially as ash particles were either hidden by ice or had already fallen from the cloud. The analysis also shows that the positions mapped by each method matched very closely with each other and with the position of the stratospheric cirrus cloud mapped with BTD and already discussed.

The SO_2 mass for the entire Hekla cloud retrieved by the various algorithms (Tables 2, 4) give values in the range of

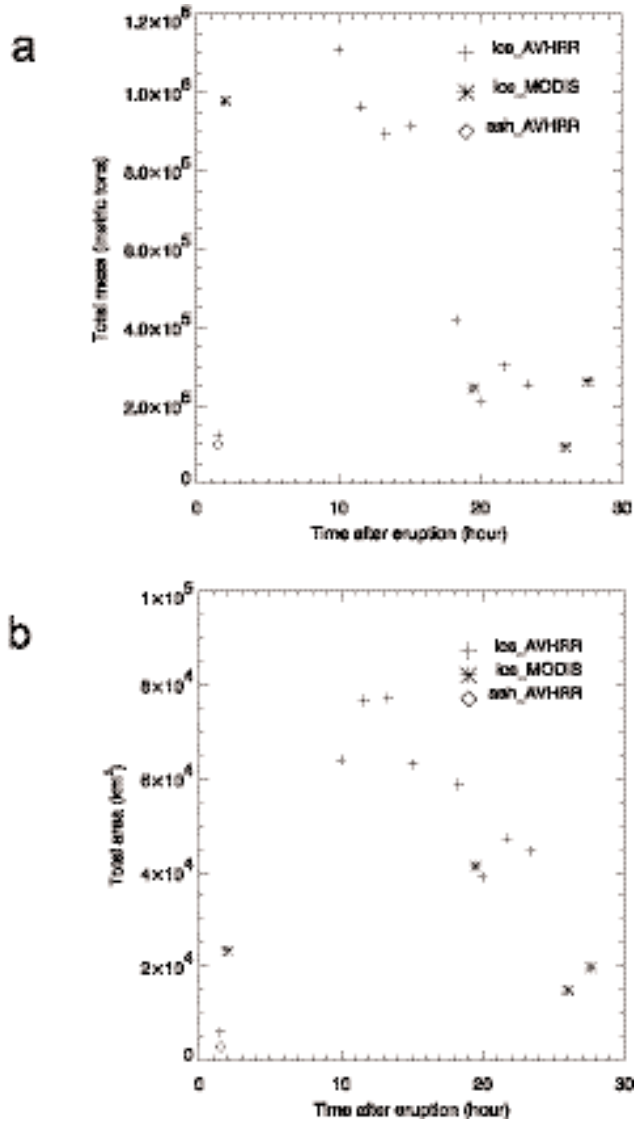

Figure 4. Fine Particle Mass and Cloud Area for Hekla Volcanic Cloud (Table 3) plotted against time after the onset of eruption. The plots crudely depict three evolutionary stages: 1. the first few hours after eruption onset when the volcanic cloud increased rapidly in size and ice mass; 2. a poorly defined intermediate stage about 10–15 hours after eruption when the cloud reached maximum area and began to decline in ice mass. At this point it was possible to track the cloud using BTD (Figure 3; Plates 1 and 2) and 3. a third stage beginning about 16 hours after eruption onset where the ice signal has faded markedly and the cloud can be better tracked by SO_2 (Plate 3, Fig 3).

0.13 to 0.37 Tg, except for the values determined on 26 February, which were much lower. We attribute the low values on the first day as being due to the very high optical depth of the volcanic cloud at that time, during the explosive venting phase of the eruption (Figures 2; Plates 4a and 5a). With a high optical depth the transmission of energy from beneath the volcanic cloud is greatly limited, and SO_2 detection is inhibited or amounts to a partial detection. This is the first time that MODIS-based determinations have been made for SO_2 so that we can compare independent results. Table 2 shows that agreement of the three methods is imperfect, yet encouraging, considering the non-optimum viewing conditions. On February 27 and 28 all estimates of SO_2 mass range from 0.1-0.3 Tg.

On Feb. 27, 2000, the Earth Probe TOMS (11:54 UT, Orbit 19683) found a very long and unusually narrow arc of sulfur dioxide extending west from southern Iceland, then north across Greenland, and finally east toward Norway (Plate 6a). The TOMS aerosol index signal on the same orbit showed no evidence of ash, but instead indicated the presence of sulfate in this very fresh cloud (~18 hrs of atmospheric residence). TOMS observed sections of the SO_2 cloud on the following two days as the cloud drifted east across the Barents Sea and south into northern Russia as shown in Plate 6b. The mass of sulfur dioxide can be determined in the more southerly portions of the cloud but retrievals near the northern terminator are very noisy because of low radiances. Thus, it is not possible to determine the total SO_2 eruption tonnage for this cloud from TOMS. We estimate that the section of the cloud shown in Plate 6a from Iceland to 74° N contained about 60 +/– 20 kt of SO_2. The analysis includes estimates from different combinations of TOMS wavelength bands.

The complete cloud found in the MODIS data of 27 February (Plates 4b and 5b) includes more SO_2 than observed with TOMS. The probable reason for the discrepancy between TOMS and MODIS is mainly due to the fact that MODIS sensed more of the cloud than TOMS. MODIS data close to the time of the TOMS overpass (see MODIS images above) indicate that a relatively large portion of the cloud was too far north and east for TOMS to measure. On the other hand MODIS appears to lose the SO_2 signal for the southern part of the plume, south of Iceland and over the Greenland ice sheet (compare TOMS images above). Thus, TOMS UV and MODIS IR data are highly complementary in unambiguous detection of plumes. There is no consistent relationship between the 7.3 and 8.6 μm retrievals, and because of the high latitude we cannot compare TOMS estimates with the others. TOMS values, which are based on scattering of solar uv radiation, are adversely affected by low solar energy of the high latitude winter season, which makes it difficult to distinguish the SO_2 signal from background noise. This problem worsened after the first day, as the cloud was located near the light terminator. MODIS values are evidently affected by cold underlying temperatures

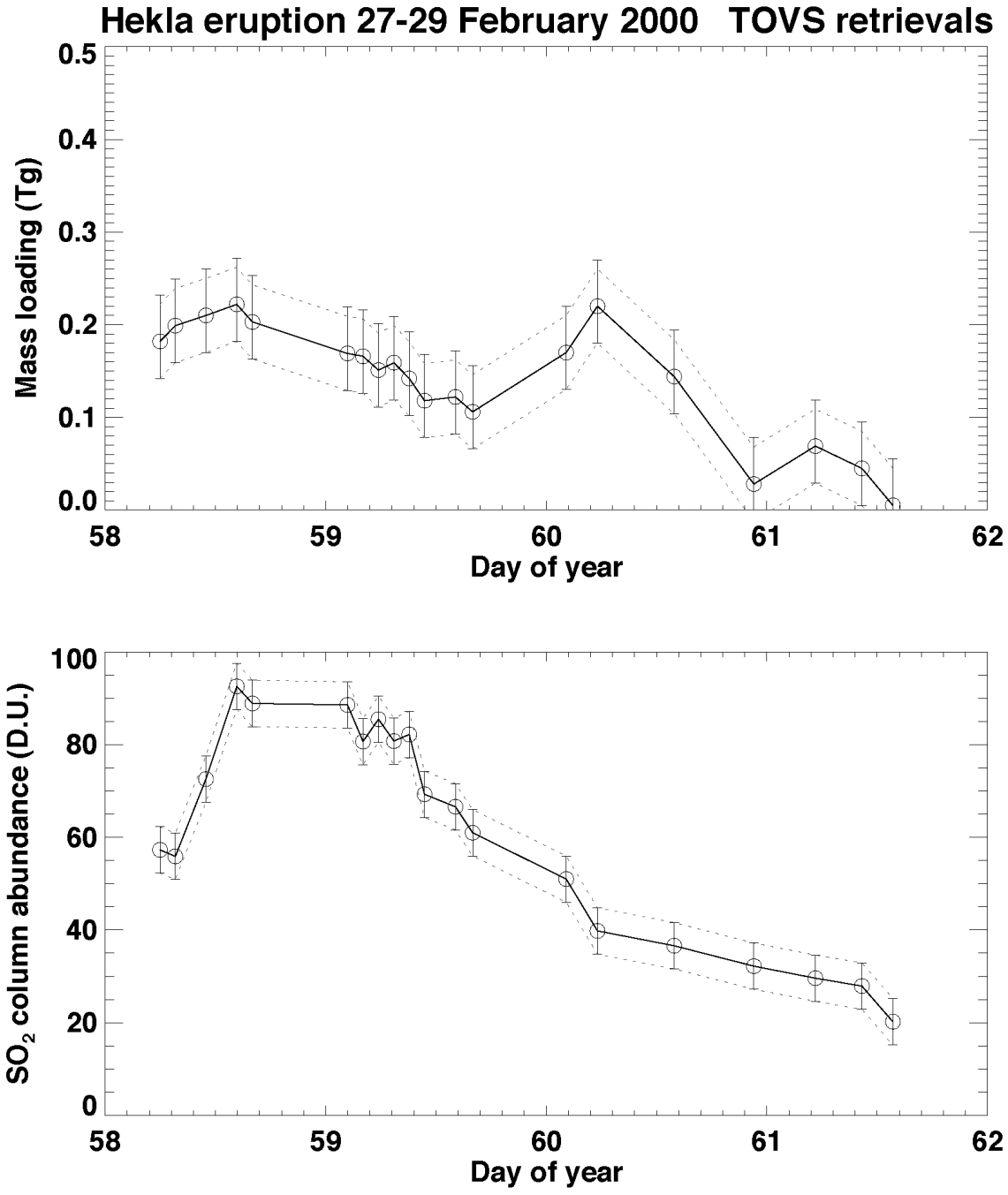

Figure 5. Plots of TOVS SO_2 retrieval data from Table 4, showing decay of mass loading of SO_2 and maximum column abundance with time (Day 58=February 27; Day 59=February 28, etc). The TOVS data on SO_2 shown extends the time of observation of the Hekla cloud beyond the data listed in Table 1, into February 29 and March 1. One interesting (and so far unexplained) feature of the data is an apparent increase in SO_2 mass on February 29.

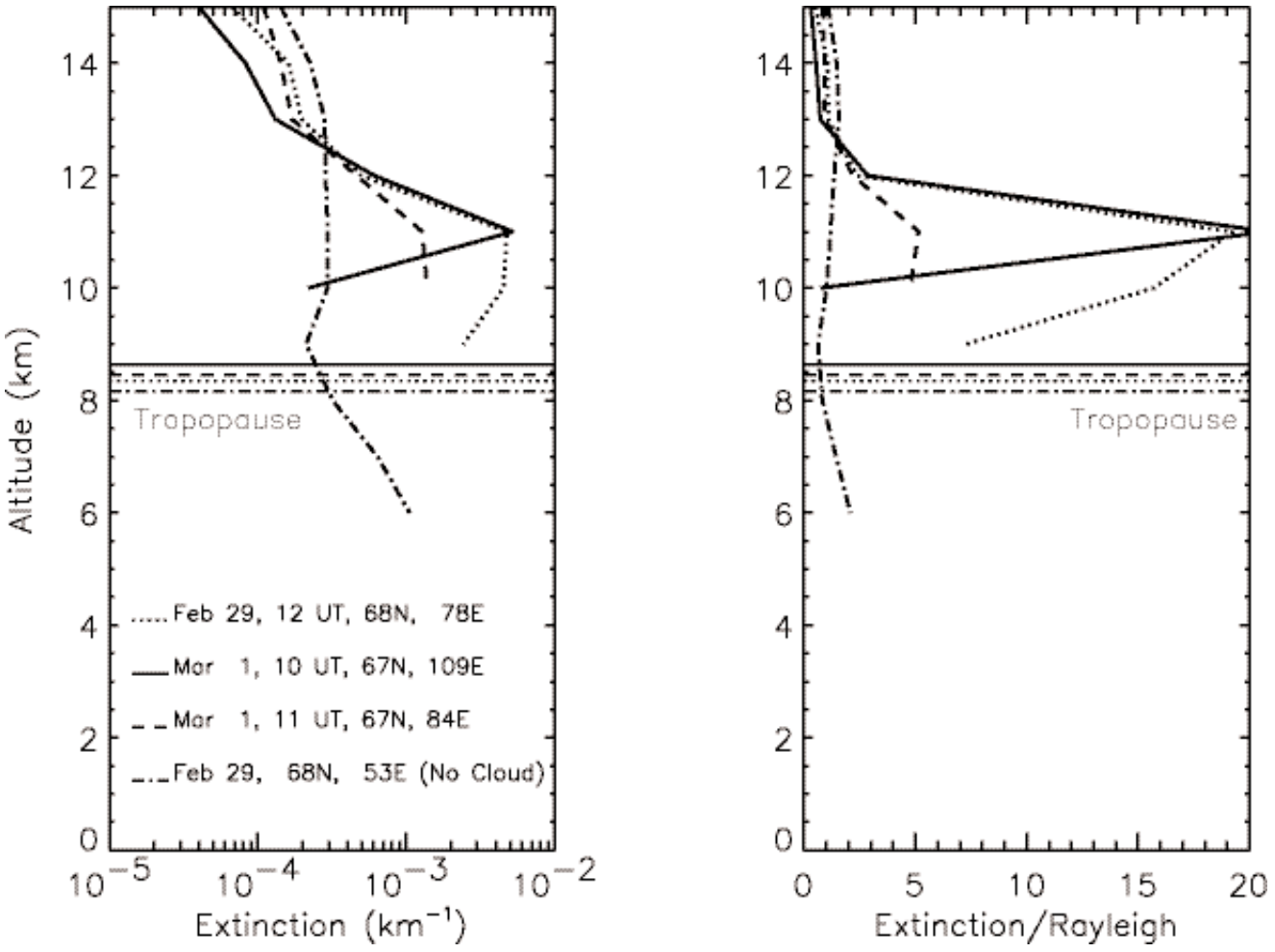

Figure 6. POAM III 1020 nm aerosol extinction and extinction ratio (Total/Rayleigh) by altitude for 29 February and 1 March 2000. These data are used to constrain the volcanic cloud height and thickness. See text for explanation.

and underestimate in these conditions, particularly when the volcanic cloud travels over Greenland (early on 27 February). It is likely that there are effects of ice on the SO_2 retrievals for both the 7.3 and 8.6 µm cases. Based on the IR transmission spectrum of ice [*Watson et al., in review*], it is likely that the 7.3 µm channel will be more strongly affected by ice, but it does not give consistently lower SO_2 as would be expected if this were the only significant environmental factor. We are only beginning to investigate the differences shown by detectors (see discussion also).

Table 2. SO_2 and sulfate mass estimates from MODIS IR and TOMS, Hekla 2000 eruption. All values in Tg.

MODIS date, time	7.3 µm SO_2	8.6 µm SO_2	TOMS SO_2	Sulfate	Revised Ice mass
26 Feb 2110	0.08	0.034	na	0.003	0.83
27 Feb 1350	0.20	0.13	0.06*	0.004	0.40
27 Feb 2155	0.17	0.37	na	0.008	0.91
28 Feb 1115	0.16	0.16-0.24		0.005	0.05

* 1139 UT; only part of the cloud sensed—<74°N portion only.

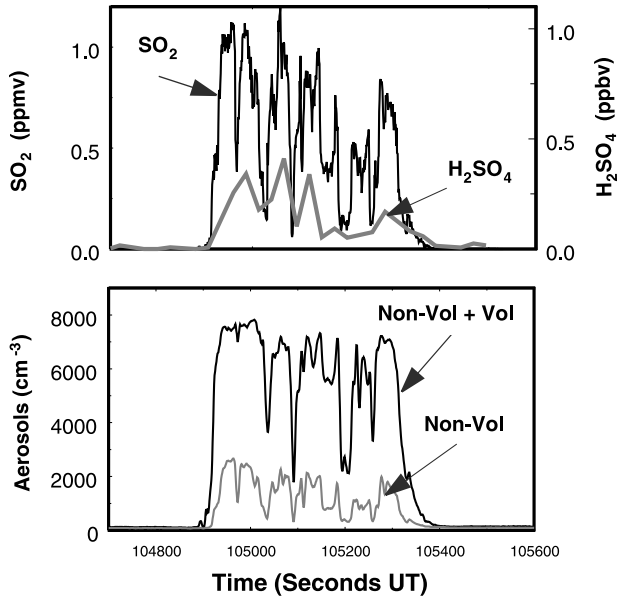

Figure 7. In-situ measurement of plume properties during the Feb. 28 DC 8 encounter at 11. 3 km altitude. The top panel shows CIMS measurements of SO_2 and H_2SO_4 and the bottom panel shows aerosol number densities in the 12–1000 nm diameter range. Both the unheated inlet (volatile plus non-volatile) and the heated inlet (non-volatile) channels are shown. The times given in the plots are in seconds starting at 0000 UT on 27 February, and amount to about 0510 UT on February 28, 2000. See text for discussion.

We used the HIRS-2/TOVS data from the same polar orbiting platform as AVHRR to retrieve the 7.3 μm data for SO_2, using the methodology of *Prata et al.,* [2003] and assuming a constant cloud height of 11 km (Table 4). These results are plotted in figure 5, and generally show agreement with the MODIS results and a gradual but not continuous decrease in SO_2 mass from just above 0.2 Tg (teragram = 10^{12} g) to 0 in about 3.5 days. The error bounds shown are determined as +/– 5 Dobson Units (milli atm cm) based on modeling errors and measurement errors. This translates into about +/– 36 kt (kiloton = 10^9 g) for a nadir pixel. The lower plot in figure 5 shows peak column abundance data, which shows a steady decline after 1400 UT on 27 February, about 7 hours after the peak in ice mass (Fig 4a). There is an increase in SO_2 mass early on 29 February, but not an increase in column abundance. We are unsure of the reason for this.

SATELLITE SULFATE AND AEROSOL DATA

A negative TOMS Aerosol Index (AI) anomaly (up to -5) was observed along the SO_2 trail on February 27 (Plate 7). This is inconsistent with volcanic ash, which would have produced a positive AI, but could have been produced by an unexpected sulfate component. This aerosol index anomaly continued on February 28 and on February 29. Non-absorbing aerosols, such as sulfate, can produce a negative AI.

Table 2 also lists the results of sulfate retrievals done with a multispectral algorithm which assumes a mixture of ice and sulfate aerosol [*Yu & Rose, 2000*]. These show aerosol sulfate masses that amount to about 2–5% of the SO_2 masses in the same cloud. Gas phase conversion to sulfate at high solar zenith angle conditions have e-folding times of ~35 days (Bluth *et al.*, 1997, p 674). Thus the results are similar to those shown for the 1982 El Chichón clouds by *Yu &*

Table 3. Ice retrievals, Hekla Volcanic Clouds of Feb 2000.

Date; time, UT	Eff Radius, μm	mean OD, unitless	Mean Burden, T/ km^2	Ice Mass, Tg	Cloud area, km^2
2/26/00; 1945	27.3	1.3	20.7	0.12	5800
2/26/00; 2100	**38.1**	**1.7**	**41.9**	**0.98**	**23000**
2/27/00; 0413	14.7	1.8	17.3	1.11	64000
2/27/00; 0554	16.7	1.1	12.6	0.96	77000
2/27/00; 0737	15.9	1.1	11.6	0.89	77000
2/27/00; 0923	18.6	1.1	14.5	0.91	63000
2/27/00; 1236	13.8	0.7	7.1	0.42	59000
2/27/00; 1350	**12.9**	**0.6**	**5.9**	**0.24**	**41000**
2/27/00; 1417	10.4	0.7	5.4	0.21	39000
2/27/00; 1557	9.3	0.9	6.4	0.30	47000
2/27/00; 1740	11.5	0.6	5.7	0.25	45000
2/27/00; 2020	**13.4**	**0.6**	**6.3**	**0.09**	**15000**
2/27/00; 2155	**20.6**	**0.9**	**13.2**	**0.26**	**20000**

Rows in **Bold type are MODIS data**; others are AVHRR, see Table 1 also.

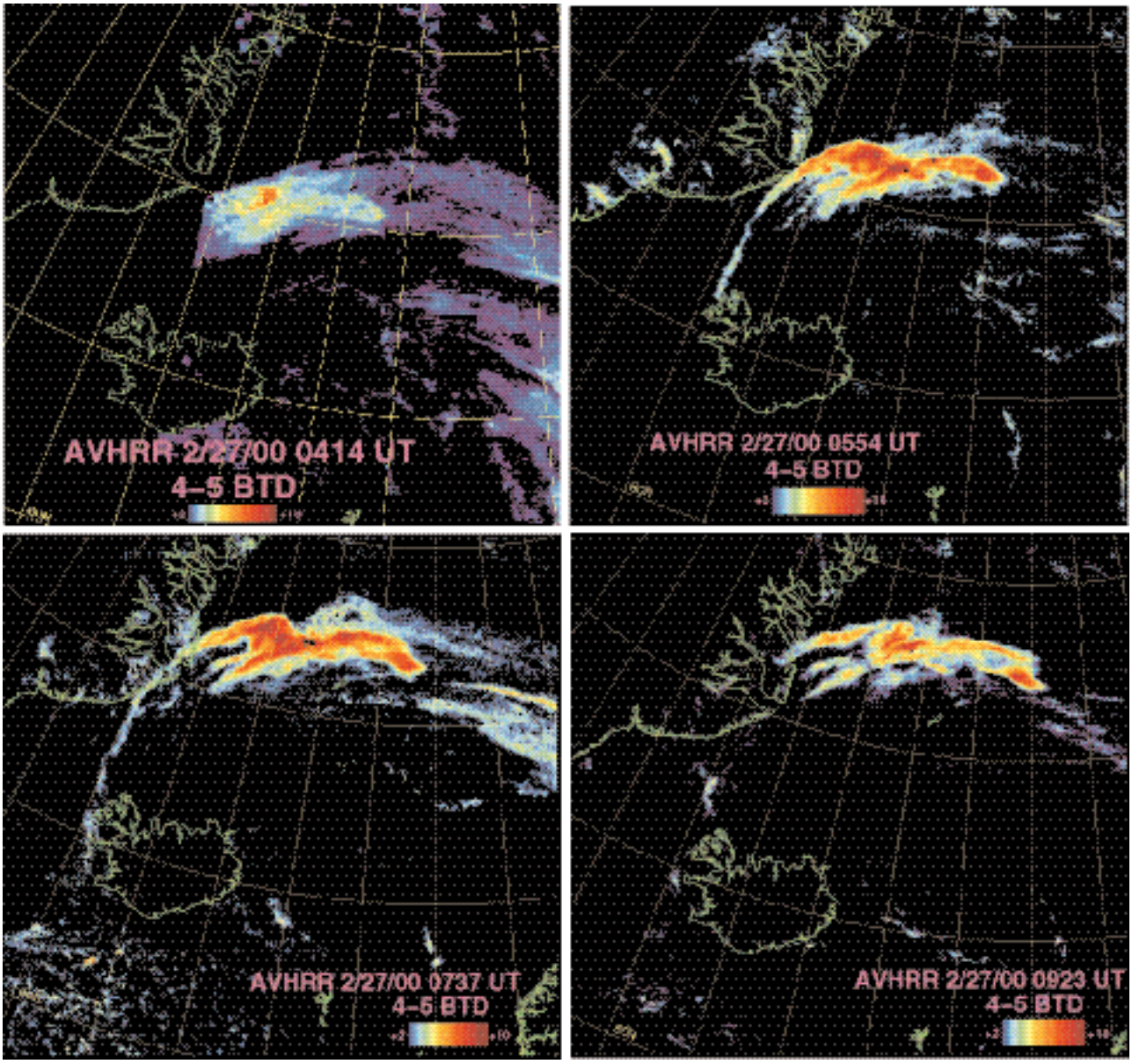

Plate 1. AVHRR images of BTD from 0414 UT (upper left), 0554 UT (upper right), 0737 UT (lower left), and 0923 UT (lower right) on Feb. 27, 2000. These depict the Hekla volcanic cloud as a high cold cirrus, gradually moving northward along the Greenland coast. The volcanic cloud at this stage is marked by positive BTD of up to +10 K and ice crystals are consistent with this. The masses and sizes of retrieved ice from these images are in Table 3.

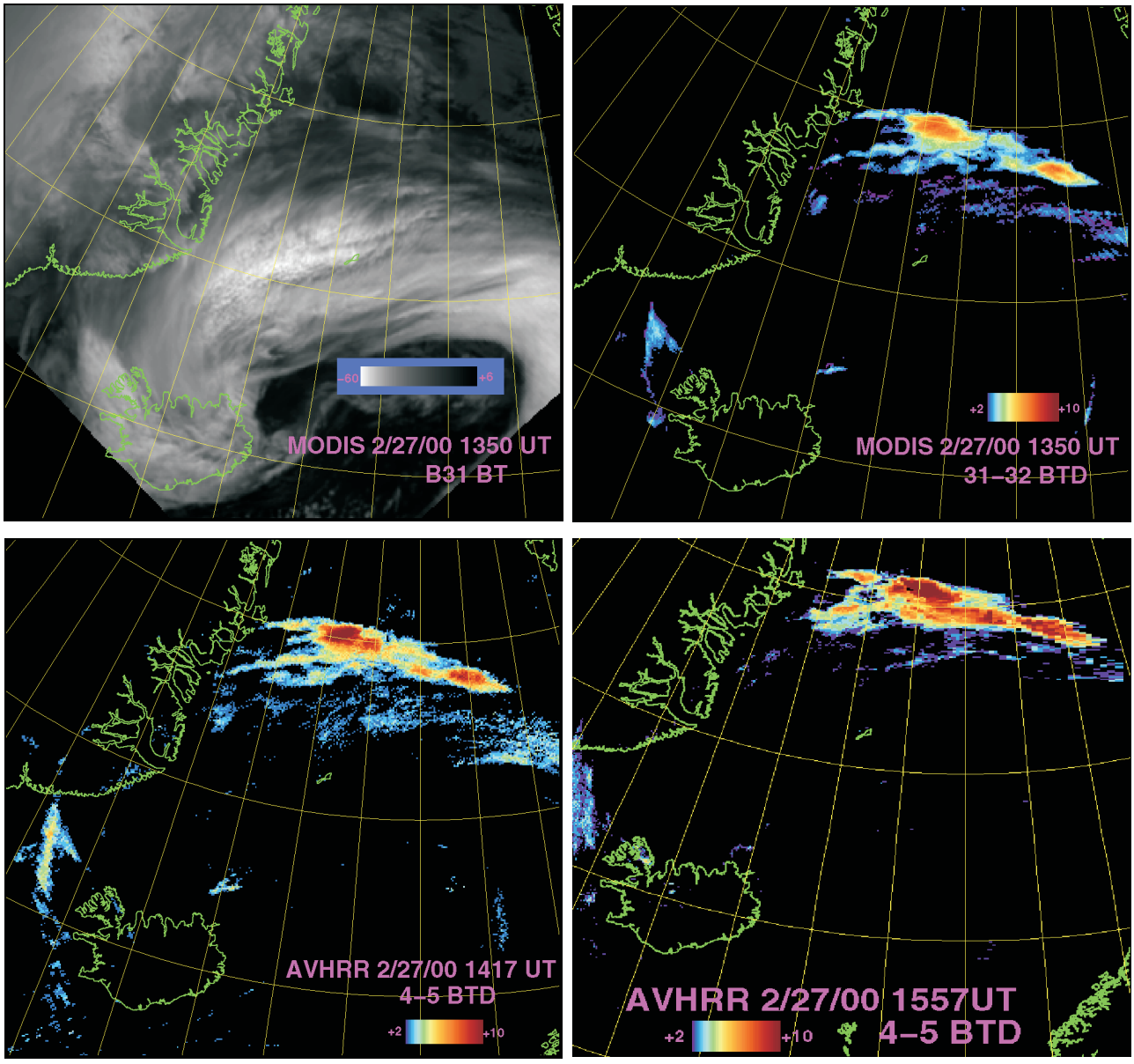

Plate 2. MODIS and AVHRR images from 27 February 2000, showing the Hekla volcanic cloud as ice masses and particle sizes are declining (Table 3, Figure 4). Upper left is a 10.7 μm BT image at 1350 UT which shows cloud patterns. Upper right is the same image in BTD, showing the position of the volcanic cloud clearly, this pair of images is about 2 hours later than the TOMS images shown in Plates 6a and 7. The lower left image is at 1417 UT and lower right at 1557 UT, and they depict slow movement of the volcanic cloud to the north. By this time the strength of the ice signal is weakening (Table 3), indicative of fallout of ice particles.

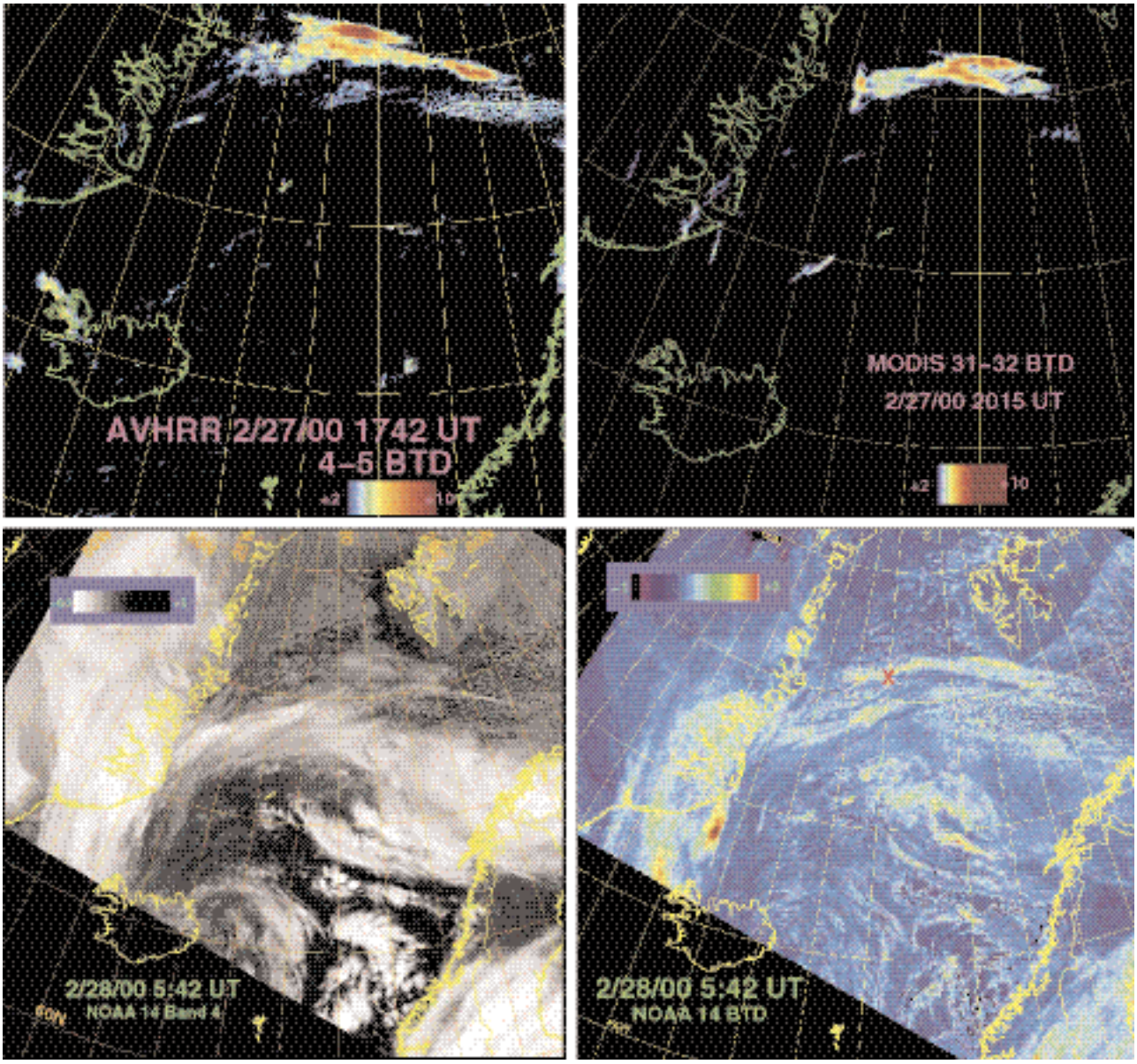

Plate 3. Satellite images from late on 27 February (upper images) and early on 28 February 2000 (lower images), showing the Hekla volcanic cloud. The upper panels are BTD representations showing the decreasing area of the discriminated volcanic cloud. The lower panels (10.7 μm BT on left; BTD on right) were acquired at 0542 UT on 28 February, about 32 minutes after the aircraft encounter. The position of the encounter, 76 N and 5 W, is marked with a red x in the lower right panel. Note that the lower right figure shows that BTD discrimination no longer can discriminate the volcanic cloud from other cirrus clouds.

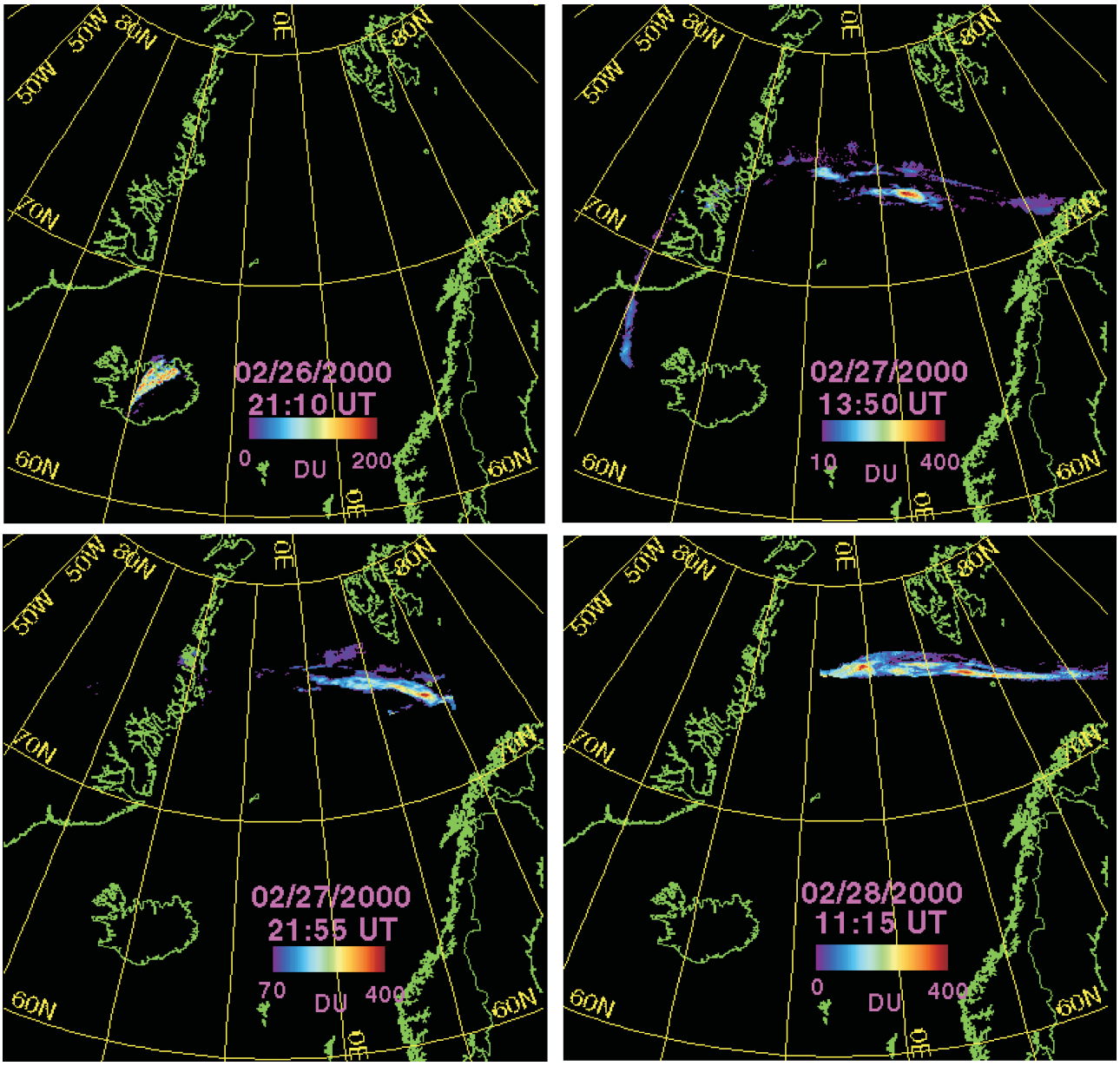

Plate 4. MODIS SO_2 sensing imagery, showing maps of the SO_2 burdens in the volcanic cloud based on the 8.6 μm algorithm [*Realmuto et al., 1997*]. These maps of SO_2 burdens can be directly compared with Plate 5, with panels in each position being equivalent. The two methods correlate well spatially but details of the comparison, made here for the first time, will be the subject of another paper. The upper right maps in both Plate 4 and Plate 5 can be compared to TOMS data collected two hours earlier (Plate 6a). The total masses of SO_2 estimated by all three algorithms are listed in Table 2.

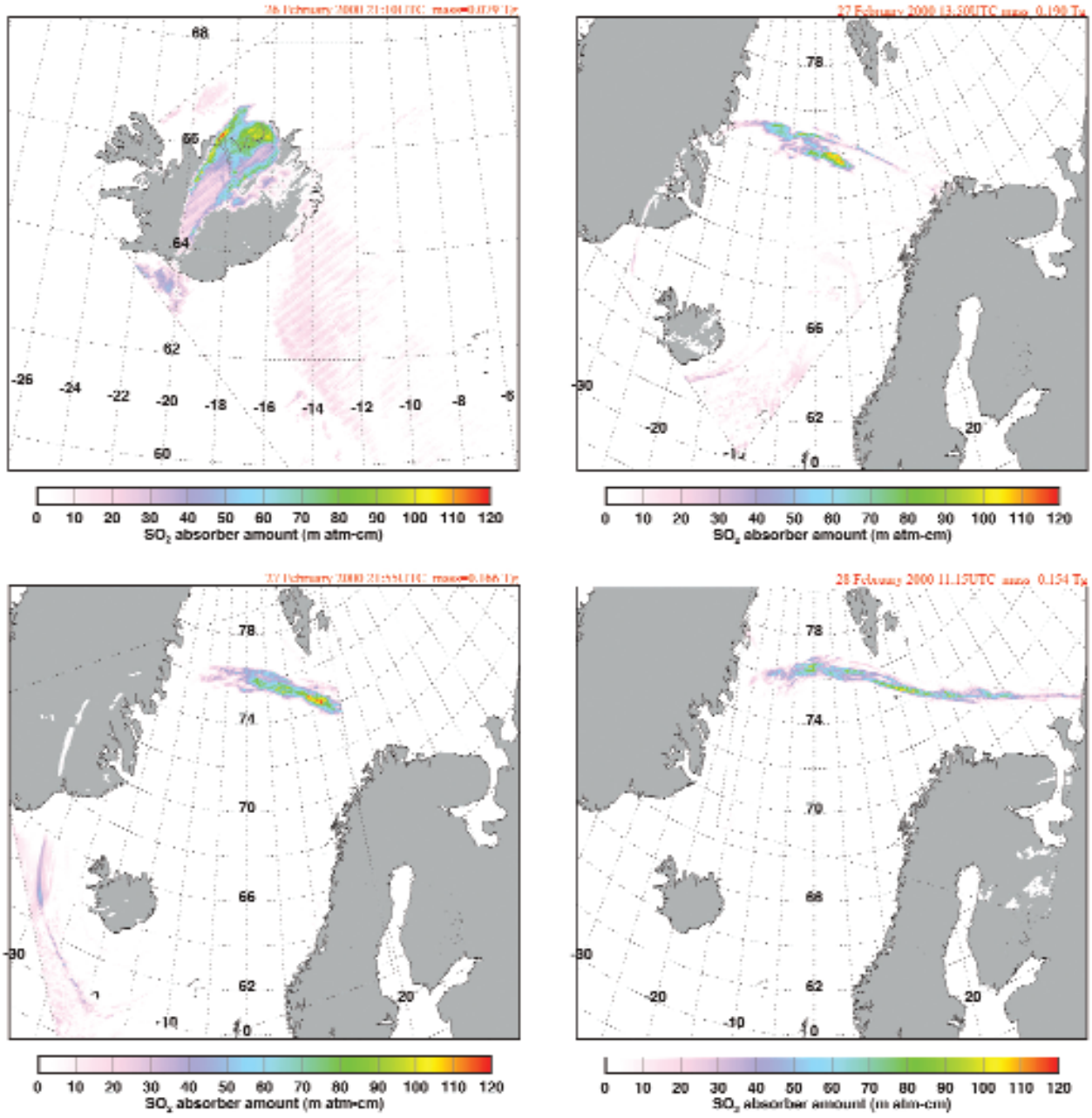

Plate 5. MODIS SO_2 sensing imagery, showing maps of the SO_2 burdens in the volcanic cloud based on the 7.3 μm algorithm [*Prata et al., in press*]. Panels show the same volcanic clouds as Plate 4.

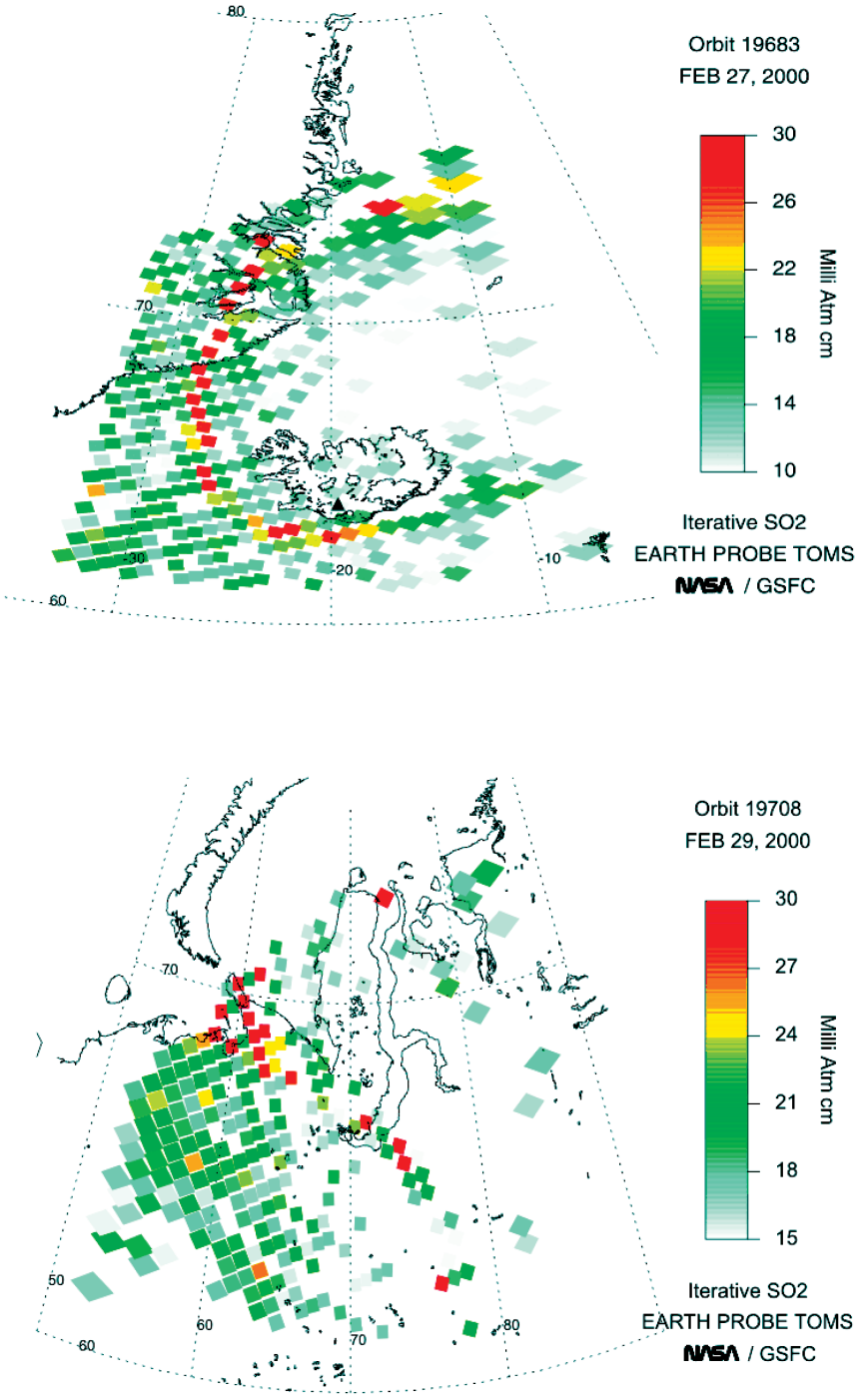

Plate 6. SO_2 burden maps of the Hekla volcanic cloud as seen by the TOMS at 1154 UT on February 27, 2000 (above) and over northern Russia on February 29, 2000 (below). Both maps use the iterative method (version 6a) of TOMS SO_2 data reduction, which is the currently preferred one. Because the TOMS measurements are adversely affected by poor solar illumination at high latitude and because the orbital coverage missed a significant part of the cloud, TOMS MODIS comparisons are not ideal (see text for discussion), but the upper panel in this figure may be compared with the upper right panels in Plates 4 and 5.

Table 4. Hekla mass loadings from TOVS data.

Day	UT	Max DU	SO_2 Tg
27 Feb	05:58	57.3	0.182
″	07:38	55.9	0.199
″	10:58	72.9	0.210
″	14:19	92.6	0.222
″	16:01	88.9	0.203
28 Feb	02:22	88.6	0.169
″	04:03	80.7	0.166
″	05:44	85.5	0.151
″	07:25	80.8	0.159
″	09:05	82.2	0.142
″	10:45	69.3	0.118
″	14:07	66.6	0.122
″	15:59	61.0	0.106
29 Feb	02:10	51.0	0.170
″	05:34	39.8	0.220
″	13:55	36.6	0.144
″	22:35	32.2	0.028
1 Mar	05:17	29.6	0.069
″	10:20	27.9	0.045
″	13:43	20.2	0.01

Cloud height assumed to be 11 km; time listed is time for pixel with largest SO_2 abundance. Areas calculated for mass loadings are equivalent space filling rectangles as projected onto earth. Error bounds are +/– % –5 DU and +/– 40 kT as shown in Fig 5.

Rose [2000] and indicate either that sulfate was formed prior to eruption or there is some (aqueous phase?) conversion of volcanic SO_2 to sulfate in the first hours to days of atmospheric residence.

POAM RESULTS

On February 29 and March 1, 2000 POAM detected enhancements of 1 μm aerosol extinction above the tropopause (Figure 6). The POAM measurements were made inside the polar vortex air mass so it is important to differentiate these aerosol clouds from polar stratospheric clouds, which POAM also detected inside the vortex near these dates. At this time the location of PSC sightings was generally near the Greenwich meridian. PSC-formation temperatures were not found near the longitudes of the POAM observations in Figure 6, which are located over far northern Siberia. To investigate the possible link with the Hekla eruption, we calculated isentropic back trajectories (not shown) from the level of the peak aerosol enhancement, which in these three cases was approximately 335 K. We found excellent corroboration between the trajectories and the location/time of the volcanic injection, thus we conclude that these aerosols were part of the Hekla plume.

The POAM data can be used to make some inferences about the spread, top, composition and thickness of the volcanic cloud. The February 29 profile was the only one that day indicating any stratospheric enhancement. POAM's coarse longitudinal sampling (roughly 25 degrees) allows us only to make the crude conclusion that the volcanic cloud had spread no further than about 50 degrees in longitude at POAM's measurement latitude (68°N) on that date. This is consistent with Defense Meteorological Satellite Program (DMSP) imagery which reveals the Hekla volcanic cloud as a narrow filament stretching from north of Scandinavia southeastward to Siberia, almost precisely to the POAM location. (DMSP shows a distinct cloud in visible imagery, but no signal in the IR. The visible cloud has impressively long shadows, confirming a very high cloud. The fact that it is invisible in the IR strongly suggests the cloud is composed of very small, hence IR-transparent, particles.) On March 1, two neighboring POAM profiles measured an aerosol layer at 11 km. These two are at 84 and 110 degrees E. Thus it appears the Hekla cloud spread out or became aligned in a meridional direction at the POAM latitude by March 1.

The POAM data, with 1-km vertical resolution, indicate

Table 5. Some infrared channels of interest on various sensors used in this study. Channels of approximately equivalent wavelength are positioned in the same row.

AVHRR		MODIS		TOVS HIRS/2	
Ch. No	center •, μm	Ch. No	center •, μm	Ch. No	center •, μm
		27	6.72	12	6.72
		28	7.33	11	7.33
				10	8.16
		29	8.55		
		30	9.73	9	9.71
4	10.7	31	11.03	8	11.11
5	12	32	12.02		
		33	13.34	7	13.35

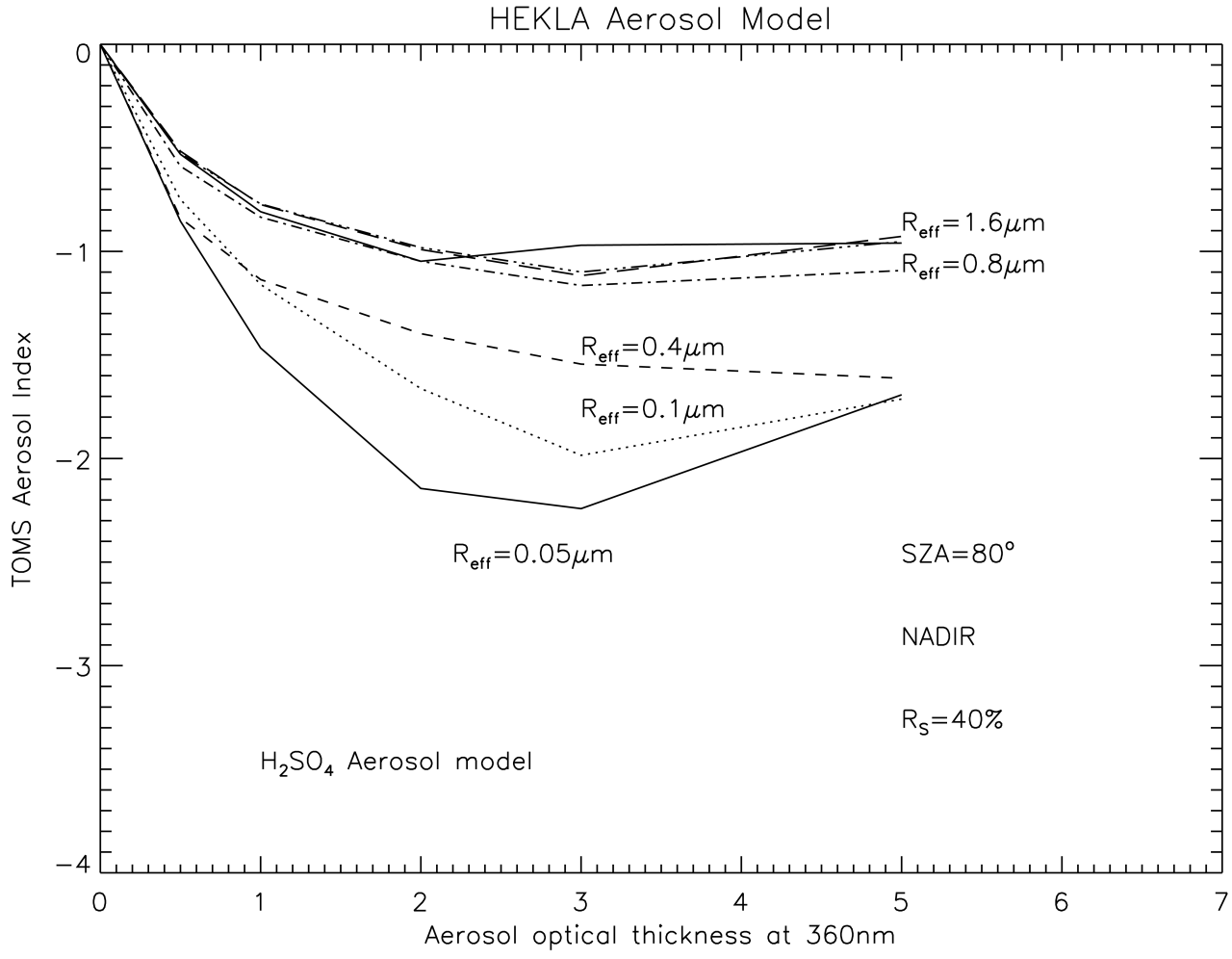

Figure 8. TOMS Aerosol Index vs. non-absorbing aerosol optical thickness at high solar zenith angles. The effect of effective radius of the particles is illustrated by the different curves. Only particles smaller than 0.05 μm will produce very negative AI values.

that the top of the plume was between 11 and 12 km. It is not possible to determine how well POAM sampled the highest portion of the cloud, but all three measurements of the Hekla cloud have the aerosol returning to "background" at 12 km. The thickness of the volcanic cloud above the tropopause may be estimated by considering that the enhanced aerosol extinction resides at all altitudes between 11 km and the tropopause (here the tropopause altitude is determined with the dynamic definition-the level at which the potential vorticity equals 3 PV Units.) The tropopause height in the three POAM cloud profiles is roughly 8.5 km. Thus the thickness of the plume in the lowermost stratosphere is on the order of 2–3 km. It is likely that the POAM profiles indicate that the depth of the cloud extends below the tropopause. Under normal background conditions, POAM can make measurements well into the troposphere (until clouds obscure the sun from the sun tracker). Figure 6 gives an example from a neighboring profile on February 29. The 3 cloud profiles all "cut off" at or above the tropopause, which indicates the presence of a cloud on the limb that is opaque to POAM. This might be cirrus or a lower portion of the Hekla cloud.

NASA DC8 ENCOUNTER

On February 28, 2000 at 0510 UT 75°N and 1°W (figure 1, Plate 3d) a NASA DC8 flying from California to Sweden crossed through the Hekla volcanic cloud [*Grindle & Burcham, 2002*]. This encounter occurred some 700 nauti-

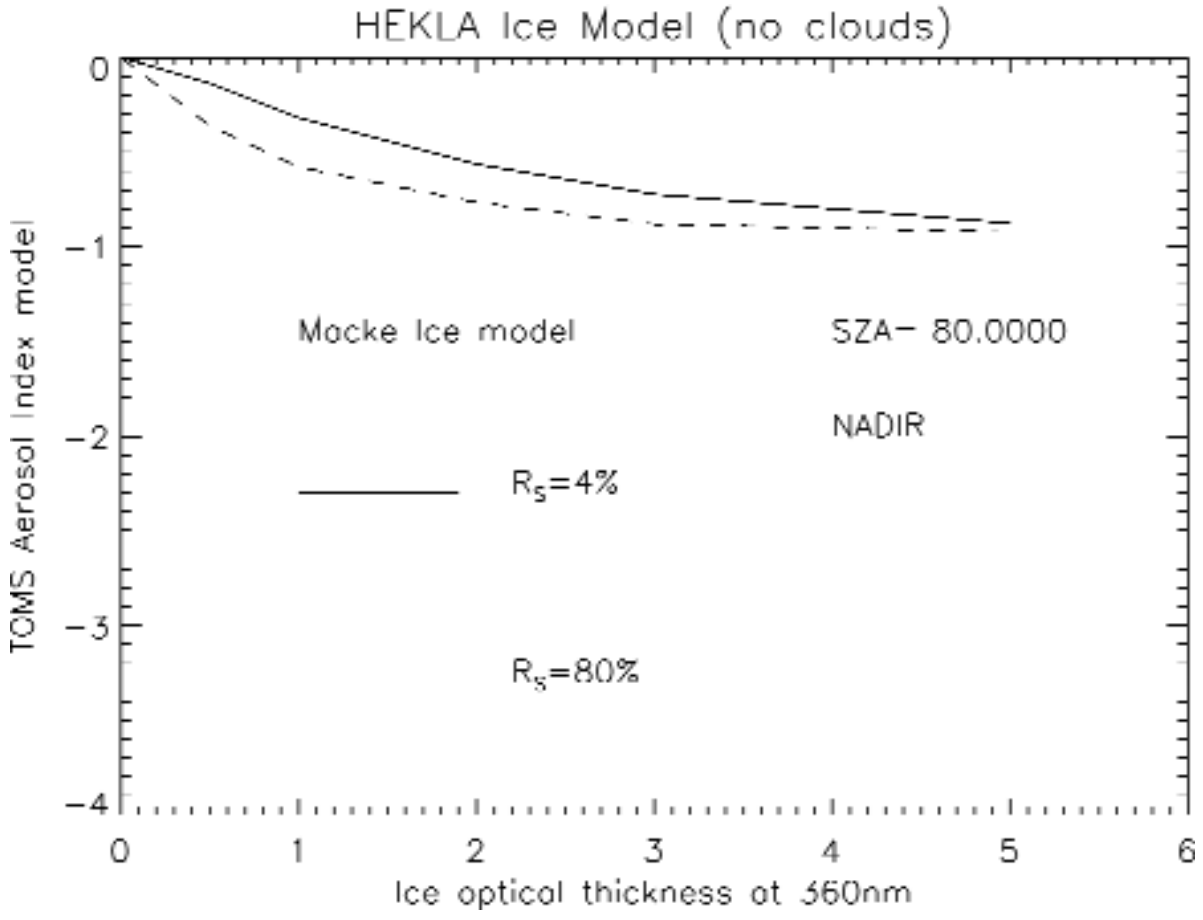

Figure 9. TOMS Aerosol Index vs. ice optical thickness for two different surface reflectivity conditions at a high solar zenith angle. No realistic amount of ice can produce the observed negative AI values.

cal miles N of the northernmost predicted position of the volcanic cloud [*Grindle & Burcham, 2002; Pieri et al., 2002*]. It was very close in time to the MODIS images shown in Plates 3c, 3d, Fig. 3, Plate 4d and 5d, and the instruments on this research aircraft collected data which are important for validation. Note that the altitude of the encounter was 11.3 km (37,000 ft.) which is near the top of the volcanic cloud, according to POAM results (see above), thus the aircraft may not have encountered the highest cloud concentrations.

SO_2, H_2SO_4 and aerosol concentrations from the 28 February cloud crossing are plotted in Figure 7. The H_2SO_4 values are upper limits to the amount in the gas phase. The timescale for each panel is seconds in Universal Time counting from 0:00 hours on 27 February; the day the flight began. The top panel shows Chemical Ionization Mass Spectrometry (CIMS) measurements of SO_2 and H_2SO_4 volume mixing ratios (VMRs). As the aircraft entered the plume the SO_2 concentration increased abruptly from the ambient level of approximately 10 pptv to 1 ppmv, an increase of approximately 5 orders of magnitude. During the 10 minutes that the DC-8 spent in the plume, numerous concentration peaks were encountered with maximum concentrations on the order of 0.5–1 ppmv, with the latter ones lower. Higher frequency, i.e. smaller spatial fluctuations, are also evident, consistent with a non-Gaussian "lumpiness" of the cloud.

SO_2 is oxidized in the atmosphere by OH forming H_2SO_4. H_2SO_4 then condenses with H_2O to form aerosols. Data from the CIMS and aerosol instruments can address the amount of oxidation. The CIMS instrument provides an upper limit to the amount of H_2SO_4 in the gas phase since aerosols can evaporate in the inlet system. The CIMS H_2SO_4 data was taken only occasionally during full mass scans of the instrument since ambient H_2SO_4 concentrations are too low to measure and the encounter with the volcanic

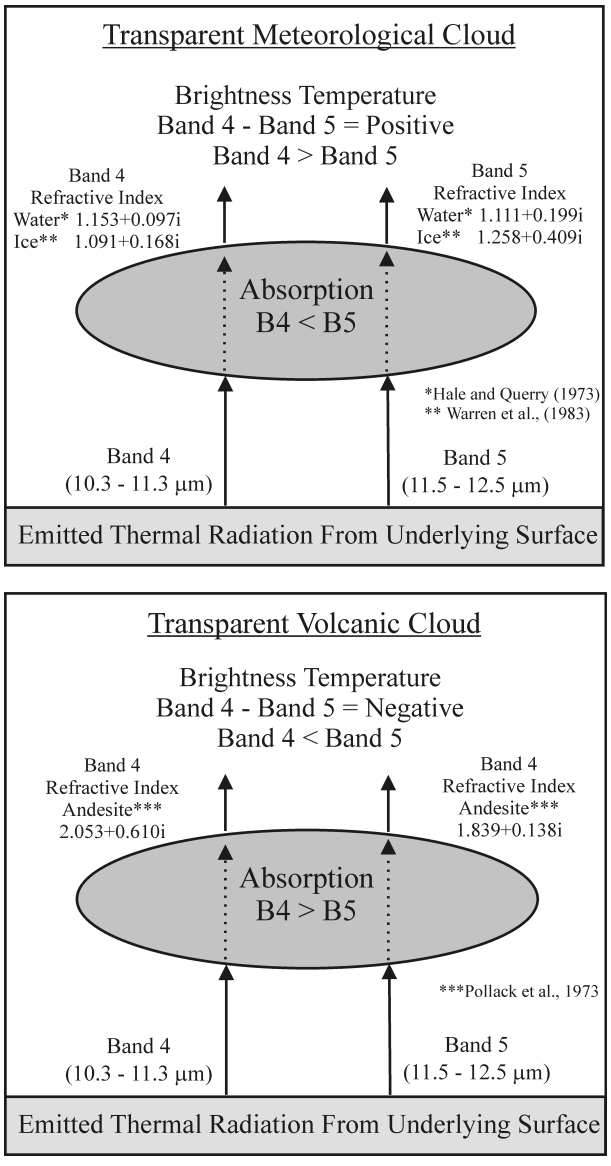

Figure 10. Schematic diagram showing how two band thermal IR transmission through meteorological and ash laden volcanic clouds is different. Bands 4 and 5 refer to AVHRR or Geostationary Operational Environmental Satellite (GOES) detectors, the equivalent bands for MODIS are 31 and 32 respectively. In the case of the Hekla volcanic clouds, which have a predominance of ice particles over volcanic ash, the response of the sensors is like a meteorological cloud.

cloud was unexpected. The peak values are on the order of 0.4 ppbv or 0.04% of the SO_2 values, indicating that little or none of the volcanic sulfur is gas phase H_2SO_4.

The bottom panel (Figure 7) shows aerosol number density data from the Langley instrument suite for aerosol particles between 12 and 1000 nm in diameter. The top trace (labeled "volatile plus non-volatile") derives from an unheated inlet line in which all aerosol particles were counted. The bottom trace (non-volatile) comes from the heated inlet in which all volatile components of the aerosol were evaporated. This portion of the measured aerosol concentration is most likely due to volcanic ash particles. A quick glance at the figure immediately shows that most of the particles were volatile. The volatile aerosols are assumed to be made of H_2O and H_2SO_4.

The amount of aerosol H_2SO_4 is derived as follows. The total aerosol volume for particles between 4 and 2000 nm diameter is calculated from the measured size distributions of the aerosol particles. Aerosol volume was converted to the mass of S in the aerosol phase using an average density for the sulfate aerosol particles of 1.68 g/cm^3 and an average bulk composition of 96% H_2SO_4 by weight (the aerosols are dehydrated in the sampling process). This calculation indicates the aerosol H_2SO_4 was 7% of the SO_2 value. This may come from atmospheric oxidation or can be viewed as an upper limit to how much is injected directly from the volcano. Note this value is at least a factor of 175 times the gas phase value. With the cold temperatures and the large surface area it is expected that any H_2SO_4 formed would condense rapidly.

Comparison of Aircraft and Satellite SO_2 and Sulfate Measurements

The concentrations of SO_2 inside the Hekla cloud were 0.5 to 1 ppmv, based on CIMS measurements (Figure 7). The burdens of the same cloud determined across transects similar to the aircraft trajectory had peak values of 100 DU and a mean of about 20 DU for the two IR algorithms. The TOMS peak values were lower (~40 DU), as would be expected from its poorer spatial resolution, but the mean was also near 20 DU. 20 DU would be equivalent to about 1 ppmv if we assume that the cloud is 2.5 km thick, consistent with the POAM results already discussed. We consider this remarkably good agreement given the fact that the aircraft crossed the cloud at an altitude near the upper limit of the cloud. The sulfate mixing ratio estimates obtained from the aircraft data (35–70 ppbv) also agree with the sulfate mixing ratio implied by the aerosol retrieval (Table 2) which is equivalent to 20–75 ppbv.

Notes on Ash and Aircraft Damages

The aircraft engines sustained significant damage from the encounter (they were all replaced), which is likely to reflect abrasive and other effects of volcanic ash [*Grindle*

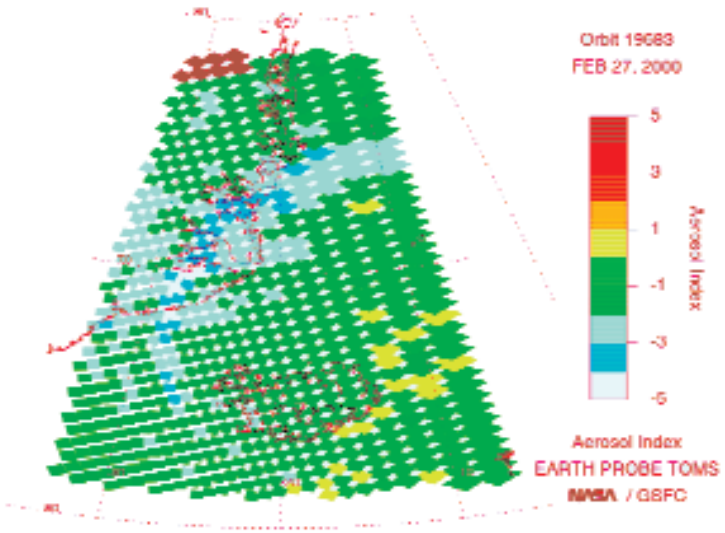

Plate 7. TOMS Aerosol Index on February 27, 2000. The blue region of strongly negative AI values, is broadly coincident with the SO_2 shown in Plate 6, upper panel. The explanation of negative AI signals is thought to be explained by the presence of sulfate particles in the volcanic cloud (see text for discussion).

& Burcham, 2002] and almost certainly corrosion by acid sulfates. We obtained samples of particles in the aircraft engines and air filters to look for ash particles. We found metallic particles and potassic feldspar fragments but no obvious volcanic ash. Another research group [*Pieri et al., 2002*] reported finding some fine ash in the air filters. This observational data is consistent with minor perhaps very fine ash being in the cloud, perhaps acting as ice nuclei, as has been the case in other eruption clouds [*Rose et al., 1995*].

DISCUSSION

We interpret the changes in ice mass in the Hekla volcanic cloud (Figure 4) to be due to the growth of ice, perhaps on ash nuclei, followed by fallout from the lower part of the cloud. The intensity of the explosive phase had strongly declined after 3–4 hours, and after 0500 UT on 27 February larger (diameter ~30 μm) ice particles were being rapidly removed from the volcanic cloud leading to the drop of retrieved ice mass beginning by about 0500 to 0900 UT on 27 February (Figure 4a, Table 3). The size of ice particles we retrieve are too small to fall to the ground in a few hours. Their effective size seems to rapidly decrease together with ice mass, so that this is also consistent with a convective instability in which the volcanic cloud separates into a gas-rich upper part and an ice-rich lower part must have occurred [*Holasek et al., 1996*] and led to fingering convection and enhanced turbulence underneath the cloud and to rapid removal of the ice [*Hoyal et al.,* 1999]. Sublimation of sinking ice would liberate SO_2 contained/trapped in ice particles and lead to enhanced column OH. This idea is consistent with observed second day increase in SO_2 (Tables 2 and 4).

Our results give us an opportunity to compare three different algorithms for SO_2 retrieval (Table 2). The masses calculated agree fairly well. TOMS results are limited and cannot be rigorously compared with the IR results: 1. TOMS missed part of the Hekla cloud outside the edge of its scan line and 2. The high latitude and winter season restricted the solar scattering, causing a high background noise. We note some differences in the three algorithms: 1. TOMS produces better results than the IR when the volcanic cloud is above Greenland, which has an unusually cold background for IR., 2. The 7.3 μm IR algorithm, seems to be affected less than the 8.6 μm by the high particle concentrations in the early Hekla cloud. Based on our testing to date we think that the 7.3 μm scheme might be more adversely affected by ice and the 8.6 μm scheme by ash. 3. The two MODIS based algorithms (7.3 μm, 8.6 μm) also deal differently with atmospheric effects. The 7.3 μm method takes advantage of the fact that atmospheric water vapor beneath the volcanic cloud is emitting IR radiation that is subsequently absorbed by SO_2 in the volcanic cloud, i.e. that it can see little of the tropospheric water vapor column. In contrast the 8.6 μm scheme sees radiation from earth's surface and must consider MODTRAN based calculations of radiative transfer through radiosonde profiles of the whole atmospheric profile. The 7.3 μm retrievals might be more accurate in high, large volcanic clouds while the 8.6 μm will do better in smaller and especially lower clouds particularly if they are ash-poor and/or water/ice rich. There are also some interesting differences, such as the much higher masses of SO_2 which are calculated from the later retrieval on 27 February (Table 2) which are of unknown cause, but possibly could be influenced by ice fallout processes which release SO_2 as suggested above. The TOVS data set (Fig 5) shows a small increase on Feb 27 (day 58) and a larger increase on 29 February (day 60), which is unexplained.

High solar zenith angle geometry cases were modeled to determine the sensitivity of the TOMS Aerosol Index (AI) to sulfate aerosols. Different conditions, such as surface reflectivity and particle size were considered. A radiative transfer model of the Hekla plume, containing small sulfate aerosols, was able to produce a negative AI signature, although not as strong as in the TOMS data.

The model shows sulfate particles smaller than 0.5 μm in radius are needed to produce a large, negative AI (Fig 8). The measured Aerosol Index (AI) is more negative than possible for larger particles. This suggests that very small aerosols were produced within the 1st day of the Hekla cloud residence or erupted with the SO_2. Ash is ruled out because it would produce a positive AI. The remaining differences are under investigation and can be associated with complex background (underlying clouds, ice surfaces, large solar zenith angles) and with the presence of ice particles in the Hekla cloud. According to the model (Fig 9) ice particles alone cannot produce the observed AI anomaly.

Our results pose questions about the relative proportions of ash, ice and gas in explosive eruptions. Ice and volcanic ash have opposing effects on upwelling thermal IR radiation (Fig 10). In other examples of recent eruptions, such as the 3 eruptions of Crater Peak, Mount Spurr, Alaska in 1992 [*Schneider et al., 1995; Rose et al., 2001*] there is an apparent dominance of ash particles as reflected by the remote sensing which features negative BTD of 10 and 11 μm IR data. Hekla's volcanic cloud is quite unlike the Spurr clouds, because it shows negative BTD only briefly and at very high optical depth (see Figure 2). We interpret this difference as being the result of abundant ice—so much ice that any ash that is present has little influence on the remote sensor. Either there are more ice particles or perhaps ice

coats ash particles, having acted as a nucleus for condensed water vapor.

We have observed other examples of ice-rich volcanic clouds: at Rabaul in 1994 [*Rose et al., 1995*] and at Soufriere Hills, Montserrat on 26 December 1997 [*Mayberry et al., 2002*]. There have been many more examples of ash-rich volcanic clouds [*Rose et al., 2000*]. In the cases of Rabaul and Soufriere Hills, it was suggested that much of the H_2O which was in the rising eruption columns came from the ocean, which evaporated extensively from contact with very hot magma. The ocean cannot have contributed to Hekla's eruption, as the volcano is miles inland and far above sea level. There is ice and snow on the volcano and some of this could have melted, but we do not judge this to have been a major source. Magmatic H_2O, which was dissolved in the magma and exsolves during magma ascent normally is released wholly or in part during eruption. In many eruptions such as the Spurr examples discussed above, the amounts of H_2O are insufficient to have produced enough ice to overwhelm the volcanic ash signal in IR sensing. Given these points, what can explain the abundance of ice in the Hekla volcanic cloud?

The mass of fine ash may have been quite limited in the Hekla volcanic cloud. We know that there was an ashfall on land in the first 3–4 hours after the eruption onset, and at least some fine ash was detected by the satellite and in aircraft filters. *Thorarinsson's* [1967] careful study of the 1947–8 Hekla eruption also described evidence for a gas-rich and ash-poor initial explosive phase. Based on the other descriptions of the Hekla activity it appears that Hekla's recent eruptions, although smaller in scale, may have started with similar early gas-rich and later gas-poor explosive phases and then evolved to effusive fissure eruptions. It is possible that degassing of magma at Hekla could have been extensive in the first 3–4 hours of activity, perhaps resulting in the loss of much of the magmatic gas from the magma erupted over the next 9 days. If gas was coming from magma staying in the system after eruption, it could be coming from a much larger volume, as much as 10 km^3 or more. We estimate, using model calculations of column dynamics after *Sparks et al.* [1997, fig 7.23, p. 206] that a 10–11 km high column could arise from about 10 Tg of H_2O at 1200°C erupted in the first hour. The total mass of magma erupted in the 9 days was about 300 Tg (0.11 km^3 dense rock equivalent volume), thus the H_2O proportion needed to degas is equivalent to about 3% of the total mass erupted.

CONCLUSIONS

SO_2 from the February–March 2000 Hekla eruption was detected by TOMS, the HIRS-2/ TOVS sensor and by two different MODIS IR algorithms, and was also measured by a NASA research aircraft. Thus we had an unusual opportunity to compare various methods. Overall the various detectors demonstrate that UV solar scattered data was affected by low sunlight of the polar winter and the IR data was affected by cold subsurfaces, particularly the Greenland icecap. Having multiple methods of SO_2 retrieval is highly advantageous because the methods each have environmental advantages under different conditions.

Hekla's eruption produced a lower stratospheric cloud to 11–12 km asl height, with up to 0.3–0.4 Tg of SO_2, up to 0.008 Tg of sulfate aerosol, >0.1 Tg of ash and >1 Tg of H_2O. The cloud resembled a high cirrus cloud. This cloud drifted north, passing over Greenland then toward Svalbard and then passing Karelia and on to Siberia in a few days. The cloud increased in ice mass throughout the explosive phase for ~10 hours and then declined after that, corresponding to migration of large ice particles to the cloud base and fallout from it after that by a convective instability of the cloud base generating rapidly sinking ice laden plumes, which may have led to ice sublimation and release of trapped SO_2. SO_2 column abundance increased in the second day and then declined after about 24 hours and was nearly undetectable after 3.5 days. With an apparent paucity of ash, the source of the cloud's buoyancy may have come from an early magmatic degassing of H_2O and other gases from magma in an explosive but ash poor phase which preceded an effusive fissure eruption of degassed magma over the ensuing 9 days.

The damage done to the NASA aircraft in spite of the paucity of ash indicates that even very small masses of airborne ash in an old and much diluted volcanic cloud more than 1000 km from its source are hazardous and should be avoided. Our data shows that such clouds can be tracked using IR data, because high cirrus cloud BTD (brightness temperature difference) detection, especially if verified with IR or UV SO_2 detection can track volcanic clouds readily, even though they show no ash signal by IR or UV. It was possible to track the Hekla cloud using AVHRR and MODIS, and new sensors such as SEVIRI (first data expected, October 2003) should have ideal capabilities [e.g. *Watkin & Ringer, 2000*].

MODIS is shown to be a robust IR sensor for volcanic clouds which can readily track the clouds progress in spite of its low ash concentration. As such the MODIS results show that new geostationary sensors which have multiple thermal IR bands, such as SEVIRI and the GOES ABI will be powerful for tracking volcanic clouds.

The Hekla example shows the value of multiple methods to monitor volcanic clouds effectively even when they are ash-poor and to advance understanding of incompletely

understood processes such as the link between fluid dynamical and microphysical processes and atmospheric chemistry modifications. The variability of volcanic clouds means that their detection must use a variety of principles and should consider that they can contain a predominance of ice over ash (or vice versa), and that they can be found in a variety of environmental conditions. The detection of SO_2, ash and ice should all be attempted and this information allows a fuller interpretation. In this case detection of ash was barely possible at all, but the tracking of the cloud using other techniques was straightforward.

Acknowledgments: This work was supported by the National Science Foundation (EAR 0106875) and by NASA. GGJE acknowledges support from the Fondation Belge de la Vocation (Golden Clover Prize). A. Hoskuldsson, H Mattson, S Kristjansson, S Karlsdottir and C Lacasse provided information about the Hekla event, Tom Grindle informed us about the DC-8 aircraft.

REFERENCES

Berk, A., L. S. Bernstein, and D. C. Robertson, *MODTRAN: A Moderate Resolution Model for LOWTRAN 7, AFGL_TR-89-0122,* U. S. Air Force Geophysics Laboratory, Hanscom Air Force Base, MA, 1989.

Bluth, G. J. S., W. I. Rose, I. E. Sprod and A. J. Krueger, Stratospheric loading from explosive volcanic eruptions, *J Geology,* 105: 671-683, 1997.

Cadle, R D and I H Blifford, Hekla eruption clouds, *Nature* 230: 573-574, 1971.

Constantine, E K, G J S Bluth and W I Rose, TOMS and AVHRR sensors applied to drifting volcanic clouds from the August 1991 eruptions of Cerro Hudson, A*GU Monograph 116—Remote Sensing of Active Volcanism,* ed by P Mouginis-Mark, J Crisp and J Fink, pp. 45-64, 2000.

Debrestian, D.J., J.D.Lumpe, E.P.Shettle, R.M.Bevilacqua, J.J.Olivero, J.S.Hornstein, W.Glaccum, D.W.Rusch, & M.D.Fromm, Preliminary Analysis of Southern Hemisphere POAM II Observations of Polar Mesospheric Clouds, *J. Geophys. Res.*, 102, 1971-1981, 1997

Ernst, G G J, J P Davis and R S J Sparks, Bifurcation of volcanic plumes in a crosswind. *Bull Volcanol* 56: 159-169, 1994.

Foster, T C and Hallett Ice crystal orientation in cirrus: Secondary torque on plate crystals in diverging electrical fields, *EOS Trans A G U* 83 Suppl: F 99, 2002.

Frogner P., S R Gislason and N Oskarsson, Fertilizing potential of volcanic ash in ocean surface water, *Geology* 29: 487-490, 2001.

Fromm, MD, R.M.Bevilacqua, J. Hornstein, E. Shettle, K. Hoppel, & J.D. Lumpe, An analysis of POAM II Arctic polar stratospheric cloud observations, 1993-1996, *J. Geophys. Res.,* 104, 24,341-24,357, 1999.

Fromm, M.D., R.M.Bevilacqua, J.D. Lumpe, E.P.Shettle, J.S. Hornstein, S.T. Massie, and K.H. Fricke, Observations of Antarctic Polar Stratospheric Clouds by POAM II in 1994 and 1995, *J. Geophys. Res.,* 102,23,659-23,672, 1997.

Fromm, M., J. Alfred, K. Hoppel, J. Hornstein, R. Bevilacqua, E. Shettle, R. Servranckx, Z. Li, and B. Stocks, Observations of boreal forest fire smoke in the stratosphere by POAM III, SAGE II, and lidar in 1998, *Geophys. Res. Lett.,* 27, 1407-1410, 2000.

Good, M Y, Cover Photo of Hekla eruption, *Geology* 29, no 6, 2001.

Grindle, T J and F. W Burcham, Jr., Even minor ash encounters can cause major damage to aircraft, *ICAO Journal,* 57: 12-30, 2002.

Grönvold, K., G Larsen, P Einarsson, S Thorarinsson and K Saemundsson, The Hekla eruption 1980-81, *Bull Volcanol* 46:349-363 1983.

Gudmundsson, A., N Oskarsson, K Grönvold, K Saemundsson, O Sigurdsson, R Stefansson, S R Gislason, P Einarsson, B Bransdottir, G Larsen, H Johannesson and T Thordarson, The 1991 eruption of Hekla, Iceland. *Bull Volcanol* 54: 238-246, 1992.

Haraldsson, K O, S G Arnason, G Larsen and J Einarsson, The Hekla eruption of 2000: The tephra fall (abstract), *25th Nordic Geological Winter Meeting,* Jan 6-9, 2000; Reykjavik, 2002.

Holasek, R E, A W Woods, and S Self, Experiments on gas-ash separation processes in volcanic umbrella clouds. J Volcanol Geoth. Res 70: 169-181, 1996.

Höskuldsson, A. and R. Ólafsdóttir. Pyroclastic flows formed in the eruption of Hekla 2000. 25th Nordic geological winter meeting, Reykjavik, 86, 2002

Hoyal D, M I Bursik, J F Atkinson, Settling-driven convection: a mechanism of sedimentation from stratified fluids, *J Geophys Res* 104: 7953-7966, 1999.

Hunton, D. E.; Ballentin, J. O.; Borghetti, J. F.; Federico, G. S.; Miller, T. M.; Thorn, W. F.; Viggiano, A. A. Anderson, B. E.; Cofer, W. R., III; McDougal, D. S.; Wey, C. C. Chemical ionization mass spectrometric measurements of SO_2 emissions from jet engines in flight and test chamber operations, *J. Geophys. Res.* 105, 26841-26856 (2000).

Jonsson, H. H. et al., *J. Ocean. Atmos. Technol.* 12, 115-129 (1995)

Krotkov, N A, O Torres, C Seftor, A J Krueger, A Kostinski, W I Rose, G J S Bluth, D J Schneider and S J Shaefer, Comparison of TOMS and AVHRR volcanic ash retrievals from the August 1992 eruption of Mount Spurr, *Geophys Res Lett.,* 26: 455-458, 1999a.

Krotkov, N.A., D.E. Flittner, A.J. Krueger, A. Kostinski, C. Riley and W. Rose, O. Torres, Effect of particle non-sphericity on satellite monitoring of drifting volcanic ash clouds, *JQSRT,* 63, 613-630, 1999b.

Krueger A J, L S Walter, P K Bhartia, C C Schnetzler, N A Krotkov, I Sprod and G J S Bluth, Volcanic sulfur dioxide measurements from the Total Ozone Mapping Spectrometer (TOMS) instruments. *J Geophys Res* 100: 14057-14076, 1995.

Mayberry, G C, W I Rose and G J S Bluth, Dynamics of the Volcanic and Meteorological Clouds Produced by the December 26, 1997 Eruption of Soufrière Hills volcano, Montserrat, W.I., in The Eruption of Soufrière Hills Volcano, Montserrat, 1995-99, ed by T Druitt and P Kokelaar, *Geological Society of London, Memoir* 21: 539-555, 2002.

Miller, T. M.; Ballenthin, J. O.; Meads, R. F.; Hunton, D. E.; Thorn, W. F.; Viggiano, A. A.; Kondo, Y.; Koike, M.; Zhao, Y. Chemical ionization mass spectrometer technique for the measurement of HNO_3 in air traffic corridors in the upper troposphere during the SONEX campaign *J. Geophys. Res.* 105, 3701-3707, 2000.

Newman, P. A. SAGE III Ozone Loss and Validation Experiment, SOLVE, A NASA DC-8, ER-2 and High Altitude Balloon Mission, http://cloud1.arc.nasa.gov/solve/; 1999.

Ólafsdóttir, R., A. Höskuldsson and K. Grönvold. The evolution of the lava flow from Hekla eruption 2000. *25th Nordic geological winter meeting,* Reykjavik, 149, 2002.

Oskarsson, N The interaction between volcanic gases and tephra: Fluorine adhering to tephra of the 1970 Hekla eruption, *J Volcanol Geoth Res* 8: 251-266, 1980.

Pieri, D., C Ma, J J Simpson, G L Hufford, T Grindle and C Grove, Analysis of in situ airborne volcanic ash from the February 2000 eruption of Hekla, *Geophys Res Lett,* 29, no 16 10.1029/2001GL013688, 2002.

Prata, A. J., Observations of volcanic ash clouds using AVHRR-2 radiances. *Int. J. Remote Sensing,* 10(4-5), 751-761, 1989a.

Prata, A. J., Radiative transfer calculations for volcanic ash clouds, *Geophys. Res. Lett.,* 16(11), 1293-1296, 1989b.

Prata, A. J., S Self, W I Rose, D M O'Brien, Global, long term sulphur dioxide measurements from TOVS data: A new tool for studying explosive volcanism and climate, EOS Trans *A G U Abstracts with Program, Spring 2002 meeting,* 2002.

Realmuto, VJ, AJ Sutton and T Elias, Multispectral thermal infrared mapping of sulfur dioxide plumes - a case study from the East Rift Zone of Kilauea volcano, Hawaii, *Jour. Geophys. Res.,* 102: 15057-15072, 1997.

Rogers R R and M K Yau, *A short course in cloud physics,* Pergamon 293 pp, 1989.

Rose, W I and G C Mayberry, Use of GOES thermal infrared imagery for eruption scale measurements, Soufrière Hills, Montserrat*, Geophys Res Lett*, 27: 3097-3100, 2000.

Rose, W I, G J S Bluth and G G J Ernst, Integrating retrievals of volcanic cloud characteristics from satellite remote sensors—a summary*, Philosophical Transactions of Royal Society, Series A,* vol. 358, pp. 1585-1606, 2000.

Rose, W. I., D. J. Delene, D. J. Schneider, G. J. S. Bluth, A. J. Krueger, I. Sprod, C. McKee, H. L. Davies and G. G. J. Ernst, Ice in the 1994 Rabaul eruption cloud: implications for volcano hazard and atmospheric effects, *Nature,* 375: 477-479, 1995.

Rose, W I, G J S Bluth, D J Schneider, G G J Ernst, C M Riley and R G McGimsey, Observations of 1992 Crater Peak/Spurr Volcanic Clouds in their first few days of atmospheric residence, *J Geology,* 109: 677-694, 2001.

Schneider, D. J., W. I. Rose and L. Kelley, Tracking of 1992 eruption clouds from Crater Peak vent of Mount Spurr volcano, Alaska, using AVHRR, in the 1992 eruptions of Crater Peak vent, Mount Spurr Volcano, Alaska, Keith, T. E. C. (Ed.), *U.S. Geological Survey Bulletin,* 2139, 220 p., 1995.

Schneider, D. J., W. I. Rose, L. R. Coke, G. J. S. Bluth, I. Sprod and A. J. Krueger, Early Evolution of a stratospheric volcanic eruption cloud as observed with TOMS and AVHRR, *J. Geophys. Res.,* 104; 4037-4050, 1999.

Seftor, C. J., N. C. Hsu, J. R. Herman, P. K. Bhartia, O. Torres, W. I. Rose, D. J. Schneider and N. Krotkov, Detection of volcanic ash clouds from Nimbus-7/TOMS, *J. Geophys. Res.,* 102: 16749- 16760, 1997.

Sigmarsson, O; M Condomines and S Fourcade, A detailed Th, Sr and O isotope study of Hekla: differentiation processes in an Icelandic Volcano, *Contr Mineral Petrol* 112: 20-34, 1992.

Smith, W. L., Woolf, H. M, Hayden, C. M., Wark, D., and McMillin, L. M., The TIROS-N operational vertical sounder, *Bull. Amer. Meteorol. Soc.,* 60, 1177-1187, 1979.

Sparks R S JM I Bursik, S N Carey, J S Gilbert, L S Glaze, H Sigurdsson and A W Woods, *Volcanic Plumes,* J Wiley & Sons, 574 pp, 1997.

Talbot, R. W.; Dibb, J. E.; Scheuer, E. M.; Kondo, Y.; Koike, M.; Singh, H. B.; Salas, L. B.; Fukui, Y.; Ballenthin, J. O.; Meads, R. F.; Miller, T. M.; Hunton, D. E.; Viggiano, A. A.; Blake, D. R.; Blake, N. J.; Atlas, E.; Flocke, F.; Jacobs, D. J.; Jaegle, L. Reactive Nitrogen Budget During the NASA SONEX Mission *Geophys. Res. Lett.* 26, 3057-3060 (1999).

Thorarinsson, S, *Surtsey: a new island in the North Atlantic.* Reyjavik Almenna Bokafelagid, 1966.

Thorarinsson, S, *The eruption of Hekla 1947-1948,* Visindafelag Islendinga, Reyjavik 1967.

Thorarinsson, S., and G E Sigvaldason, The Hekla eruption of 1970, *Bull Volcanol* 36: 269-288, 1972.

Viggiano, A. A. D. E. Hunton, Airborne Mass Spectrometers: Four Decades of Atmospheric and Space Research at the Air Force Research Laboratory, *J. Mass Spectrom.* 34, 1107-1129 (1999).

Wallace, J M and P V Hobbs, *Atmospheric Science: An introductory Survey,* Academic Press, 1977.

Watkin, S and M A Ringer, Investigation into the use of SEVIRI imagery for the automatic detection of volcanic ash clouds. UK Met Office *NWP Forecasting Res Tech Rep No* 297, 2000.

Watson, I. M., V. J. Realmuto, W. I. Rose, A. J. Prata, G. J. S. Bluth, Y. Gu and T. Yu, Thermal infrared Remote Sensing of Volcanic Emissions using the Moderate Resolution Imaging Spectrometer (MODIS), *J. Volcanol Geoth. Res.* in press.

Wen, S and W I Rose, Retrieval of Particle sizes and masses in volcanic clouds using AVHRR bands 4 and 5, *J. Geophys. Res., 99*:5421- 5431, 1994.

Yu, T and W I Rose, Retrieval of sulfate and silicate ash masses in young (1-4 days old) eruption clouds using multiband infrared HIRS/2 data, *AGU Monograph 116 —Remote Sensing of Active Volcanism,* ed by P Mouginis-Mark, J Crisp and J Fink, pp. 87-100, 2000.

William I. Rose Geological Engineering & Sciences, Michigan Technological University, Houghton, MI 49931 USA raman@mtu.edu

Yingxin Gu Geological Engineering & Sciences, Michigan Technological University, Houghton, MI 49931 USA yigu@mtu.edu

I. Matthew Watson Geological Engineering & Sciences, Michigan Technological University, Houghton, MI 49931 USA watson@mtu.edu

Gregg J. S. Bluth Geological Engineering & Sciences, Michigan Technological University, Houghton, MI 49931 USA gbluth@mtu.edu

A. J. Prata CSIRO, Atmospheric Research, Aspendale, Victoria, Australia Fred.Prata@csiro.au

Arlin J. Krueger JCET/UMBC 1000 Hilltop Circle Baltimore, MD 21250

Nikolai A. Krotkov krotkov@chescat.gsfc.nasa.gov

Simon Carn JCET/UMBC 1000 Hilltop Circle Baltimore, MD 21250 scarn@umbc.edu

Michael D. Fromm Computational Physics, Inc; 8001 Braddock Road Suite 210 Springfield, VA 22151 mike.fromm@nrl.navy.mil

Donald E. Hunton Air Force Research Laboratory, Space Vehicles Directorate, Hanscom AFB, MA Donald.Hunton@hanscom.af.mil

Gerald G. J. Ernst, CEGF, Earth Sciences, University of Bristol, UK, gerald.j.ernst@bristol.ac.uk

A. A. Viggiano, Air Force Research Laboratory, Space Vehicles Directorate, Hanscom AFB, MA 01731 USA Albert.Viggiano@hanscom.af.mil

T. M. Miller, Air Force Research Laboratory, Space Vehicles Directorate, Hanscom AFB, MA 01731 USA Thomas.Miller@hanscom.af.mil

J. O. Ballenthin, Air Force Research Laboratory, Space Vehicles Directorate, Hanscom AFB, MA 01731 USA balleuthin@plh.af.mil

J. M. Reeves, Engineering Department, University of Denver, Denver CO 80208, jreeves@du.edu

J. C. Wilson, Engineering Department, University of Denver, Denver CO 80208, jwilson@du.edu

B. E. Anderson, NASA Langley Research Center, Hampton, VA b.e.anderson@larc.nasa.gov

D. E. Flittner, Atmospheric Sciences, University of Arizona, Tucson, AZ 85721 flittner@atmo.arizona.edu